UNIVERSITY OF OKLAHOMA

GRADUATE COLLEGE

INFERRING INTERWELL CONNECTIVITY BY STATISTICAL DIAGNOSTIC TOOLS AND SIGNAL PROCESSING METHODS

A THESIS

SUBMITTED TO THE GRADUATE FACULTY

in partial fulfillment of the requirements for the

Degree of

MASTER OF SCIENCE

By

YAO WANG
Norman, Oklahoma
2018

INFFERING INTERWELL CONNECTIVITY BY STATISTICAL DIAGNOSTIC TOOLS AND SIGNAL PROCESSING METHODS

A THESIS APPROVED FOR THE
MEWBOURNE SCHOOL OF PETROLEUM AND GEOLOGICAL ENGINEERING

BY

Dr. Zulfiquar Reza, Chair

Dr. Deepak Devegowda

Dr. Xingru Wu

Acknowledgements

I would like to sincerely express my appreciation to my advisor, Dr. Zulfiquar Reza, for his help and support throughout my graduate studies at the University of Oklahoma. I'm grateful for his guidance, advices, and encouragement, which makes it possible for me to complete my degree and explore limitations and potentials for my life. I'm also grateful for his patience and dedication in reviewing my research and this thesis.

I extend my sincere thanks to Dr. Deepak Devegowda and Dr. Xingru Wu, for participating in my committee and providing comments and suggestions for my presentation, defense and thesis; for lecturing great courses that make me learn more than textbook knowledge.

I would like to express my gratitude to my coworkers and friends, Tien Phan, Any Ordonez, Ziyi Xu, Jing Zhang and Changqing Yao, for their encouragement and accompany throughout my graduate study.

I am grateful to Schlumberger and MathWorks for donating Petrel and Matlab license; MPGE department for granting me graduate assistantship.

Finally, I would like to particularly thank my mom Ping Huang, my dad Xiaoqiang Wang, my boyfriend Philip Babb and his family for giving me endless love and support.

Table of Contents

List of Table

List of Figures

Abstract

Data mining has become increasingly crucial in deciphering reservoir dynamics. Operators currently acquire an enormous amount of data that are not effectively being used. These data contain valuable information about subsurface processes. Interwell connectivity is one of the most significant aspects of subsurface characterization that can impact a project's success. In this thesis, I present novel techniques to quantify and monitor interwell communication by applying signal-processing methods to observed and derived well-based measurements and variables.

I construct a suite of realistic reservoir models under varying conditions involving multiple producing and water-injection wells. More than 40 static and dynamic parameters including permeability, porosity, water saturation, fluid properties and rock-fluid interaction terms are varied using experimental designs to capture realistic uncertainty. Waterflood scenarios are modeled using streamline simulation to infer injector-producer pair connectivity, pattern allocations, drainage efficiency, and their evolution. These injector-producer variables are analyzed using numerous signal-processing methods including cross-correlation, time-lag correlation coefficient, coherence, and periodogram, among others. Well variables examined involve pressure, rate, and their derivative functions.

I employed a thorough and systematic multipronged approach to decipher signals of the injector-producer well variables. At one level, the objective was to identify which variables pair provides meaningful connectivity information. Combination of well variables examined includes injector bottom-hole pressure (BHP) – producer BHP; injection rates – production rates; injector productivity index (PI) – producer PI; injector

well variables – producer gas-oil ratio; and $F1 - F2$. Here, $F1$ is a producer well-variable defined as the production rate added to the product of PI and BHP of the producer, while $F2$ is simply the difference between injection and production rates.

The other objective was to identify which signal-processing technique(s) will be most useful to infer interwell connectivity. To verify well connectivity, I used pair-wise allocation values based on streamline simulation. Our analyses indicate cross-correlation of $F1 - F2$ contains most meaningful connectivity information. In this context, I have also compared the performance of our approach with the capacitance-resistance model for validation. A large dataset from the Permian Basin constituted the primary content of this investigation.

I examined and devised several signal-processing techniques of well variables to assess interwell connectivity in realistic reservoir settings. The approaches reveal new insights into determining reservoir communication metrics. The proposed methods can be easily implemented in the automated virtual flow-metering system. These methods will help identify the predominant injector-producer pairs and make operational decisions at any stage of waterflood or enhanced-recovery projects.

Chapter 1: Introduction

This thesis presents work performed for a Master of Science degree that was conducted at Mewbourne School of Petroleum and Geological Engineering of the University of Oklahoma. The research presented herein develops novel techniques to infer well connectivity in waterflood reservoirs.

1.1 Motivation and Problem Statement

Waterfloods have been the most widely used secondary recovery technique in conventional reservoirs. In any such recovery process involving water injection, understanding the flow efficiency between the injection and the producing wells becomes paramount, which leads to the study of interwell connectivity between an injector and a producer. This interwell connectivity directly affects the conformance or the uniform progression of the injection front in flooding operations. Among other items, conformance depends on the interwell communication. Interwell connectivity is typically determined by analyzing the injection and production rate and pressure data.

Previous studies have provided multiple methods to infer connectivity between wells. Prior to 2000, the studies mostly relied on statistical tools, such as Spearman rank, Pearson's correlation coefficient and similar diagnostics, as discussed by Tian and Horne (2016). A high correlation coefficient within the injector-producer rates or pressure data usually implies a strong connection between the well pairs (injector-producer). Many reservoir and pilot studies rely on tracer tests to infer the interwell communication (Morales et al. 2018, Poulsen et al. 2018, Tiong-Hui and Cheng 2018). Integration and acquisition of sophisticated crosswell time-lapse electromagnetics (Wilt et al. 2012, Biterge et al.

2014), acoustics (Danaei et al. 2018) and gravity sensors (Meyer 2008) data can also help decipher interwell communication.

In recent years, with the upwelling development of simulators, model-based approaches combine robust analytics with a rigorous description of subsurface architecture yielding an improved picture of interwell connectivity (Albertoni and Lake 2003, Yousef et al. 2006, Dinh and Tiab 2008, Sayarpour 2008, Sayarpour et al. 2009, Hou et al. 2012, Mirzayev et al. 2015, Mirzayev and Jensen 2016). Using injection and production data, Albertoni and Lake (2003) formulated a constrained linear multivariate regression (MLR) approach to obtain weight factors between injectors and producers as indicators of connectivity. They used liquid production and injection rates and diffusivity filters established by static reservoir properties. They concluded that connectivity between wells depends on the relative distance of wells and geological property variations but are independent of injection and production rates. One of the limitations of this study is that this approach ignores transient data as well as the data during shut-in periods. Yousef et al. (2006) improved the MLR approach by introducing the capacitance model replacing the diffusivity filters with time constants. The resulting connectivity indices and time constants can represent reservoir and fluid properties between injectors and producers. In a subsequent study, Sayarpour (2008) developed capacitance-resistance model (CRM), which can use injection rates even with shut-in periods, production rates that have remnant primary production and bottom-hole pressure (BHP) data if available. Around the same time, Dinh and Tiab (2008) introduced a procedure to determine interwell connectivity based on fluctuations of BHP for both injectors and producers. The method utilized the

same idea of MLR, but with pressure data. Their method avoids the use of diffusivity filters and does not exclude transient data unlike the MLR approach of Albertoni and Lake (2003).

In this thesis, I explored in a systematic manner several signal-processing techniques probing the fluctuations of well-based variables with an aim to infer interwell communication. This study, at present, provides a suite of formative approaches involving multiple well-variable pairs between injector and producer pairs using the signal-processing techniques. The well variables examined include fluctuations of injection and production rates, bottom-hole pressure and their derivative functions.

1.2 Objective

The objectives of the study are the following:

(1) Examine and devise several signal-processing techniques.

(2) Identify informative well data to provide information of communication between injectors and producers over time.

(3) Deduce connectivity measures and systematically evaluate their efficacy in characterizing subsurface connectivity picture.

1.3 Organization of Thesis

Chapter 2 reviews relevant literature. This provides previous studies on the investigation of interwell connectivity, using direct methods, statistical tools, or model-based tools.

Chapter 3 introduces several digital signal-processing techniques with the definitions, mathematical functions, and example profiles. These techniques include: cross-

correlation coefficient, magnitude-squared coherence, and periodogram. The indicators based on the profiles of these techniques are also presented.

Chapter 4 provides the investigation on two-well scenarios for the digital signal-processing techniques illustrated in Chapter 3. I constructed reservoir models under various conditions in order to identify the effect of well distance, layer-wise zonation, well interference, and heterogeneity. For these conditions, I examined the efficacy of the signal-processing methods and the associated connectivity indicators. From this exercise, I identified the most informative method and well-variable pairs at the end of the chapter.

Chapter 5 provides the investigation of signal-processing techniques under complex realistic multi-well reservoir scenarios. Based on the observations from Chapter 4, I applied the most effective signal-processing methods and connectivity indicators to over one hundred realistic heterogeneous reservoir scenarios. These reservoir scenarios are built by various Design of Experiment matrix of reservoir properties.

Chapter 6 is a comparison study for the proposed method to streamline simulated responses. I generated streamline rates and injector-producer allocation fractions based on numerical simulation runs. I consider these simulated responses as the truth cases. I statistically compared the performance of the proposed connectivity indicators using over one hundred uncertainty cases. A suite of scatterplots and heatmaps are presented to show the comparison results.

In Chapter 7, I compared the performance of the proposed connectivity indicators against Capacitance-Resistive Model, one of the most popular methods in recent years for inferring interwell connectivity. CRM determines the communication strength between

each injector and producer pair. I compared the CRM connectivity measures with the indicators proposed in this study.

Chapter 8 discusses the limitations and the strengths of the connectivity indicators and lastly concludes this research.

Chapter 2: Literature Review

Reservoir connectivity is a critical component of reservoir performance evaluation and management. It is one of the key issues in understanding the dynamic field performance, especially during a waterflood process. There are direct and indirect methods to characterize reservoir connectivity between wells. Among them, the direct methods include tracer testing, geochemical fingerprinting, pressure-transient testing etc., that provide opportunities to quantify the reservoir connectivity. However, there is no direct measurement to evaluate well-to-well connectivity.

In order to characterize the communication between wells in a reservoir, researchers have been coming up with various approaches through the years, using statistical tools, numerical simulations and signal-processing techniques. This chapter will provide a literature study of the historical developments of the methods that measure and quantify connectivity between wells.

2.1 Direct Methods for Measuring Connectivity

Tracer and transient testing are usually the direct methods to quantify reservoir connectivity.

The application of waterflood tracers is based on the assumption that the movement of the tracer can reflect the movement of the injected water. The results hold true if the properties of the tracer meet the constraints of the formation, so that the tracer would follow the injected water without significant loss or delay. Under the conditions where there are more sources for water to enter, for example, formation water and water from different injection wells in the same field, tracer testing is the viable mean to distinguish between them (Zemel 1995).

Well testing is a crucial technique to obtain reservoir properties. Interference test and pulse test are commonly used for determining the communication between two wells. They are designed to determine the reservoir properties like permeability in the interwell region. Interference test contains creating a significant pressure disturbance in one well, and measuring pressure response in another well. The pulse test is to send a coded signal from an active well to a shut-in observation well. However, for a massive waterflooding field, this kind of test could be difficult to conduct since the signal can be distorted by the other wells. And also, the observation well requires repeat sequence of shutting-in and producing. (Lee et al. 2003)

Both the tracer tests and the pressure-transient tests provide great aid with determining the flow path preference and water breakthrough time in a waterflood reservoir, as a clue for reservoir connectivity information. However, as Ohno et al. (1987) has mentioned, both of the tests require considerable time. The well-to-well transient tests need to last long enough in order to see the pressure change, whereas the tracer tests need longer time for the fluid flow to be seen from well to well. They concluded that both of the tests are complement to each other. And they showed a comprehensive study of their applications and limitations.

Because of the large time requirements and the limitations of these direct methods, engineers tempt to deduce interwell connectivity information from the production data obtained. This avoids the need to shut-in the well that causes loss of production. The following sub sections provide the literature study of these attempts.

2.2 Statistical Tools for Inferring Interwell Connectivity

Heffer et al. (1995) used Spearman rank correlation in rates between injectors and producers to reflect communication through the reservoir. The study concluded that the signal passed between wells have some component coupled to geomechanics features. During the application to several waterflooding field involved large number of well pairs, spurious negative correlations has occurred occasionally. It was suggested that these negative correlations were caused by geomechanical change, well interference, early water break-through or isolated compartments. A lag-time between injector and producer time serious has been introduced to the investigation, but it failed to give systematic behavior correlations. Thus, the applications were conducted without lag.

Refunjol et al. (1996) combined reservoir geology, tracer data and Spearman rank correlation coefficient analysis of injector/producer rate data to assess information about reservoir continuity in interwell regions. They investigated the effect of nonzero time lags between injector-producer pairs, extended to previous Spearman rank applications with zero time lag by Heffer. They were able to infer preferential flow directions by the information provided by the rank correlation. However, they concluded that there were considerations remained to use Spearman technique by itself, such as fluid compressibility in the correlations, accounting for multiple-well correlation, and explanations for correlations at distance.

Jansen and Kelkar (1997) have shown how the cross correlation between rate performance of pair of wells can give information about the flow path pictures in the subsurface. But because of the complex nature of interwell relationship, the calculation was problematic. The time serious being non-linear and non-stationary violated their

stationary assumption. They addressed that the noise in the data, pressure superposition and poor mass balance also caused difficulties in processing the data. Coherently, they investigated the wavelet transform in order to break down the data into frequency spectra in order to provide treatment to the non-stationary data. They illustrated the usefulness of this tool and concluded that it is necessary to capture the transient nature of cross correlation, and its success depends upon the treatment of data.

Panda et al. (1998) developed an artificial neural network method to estimate well interaction, such as faults, pinchouts, regional permeability trends etc. between different well pairs within a pattern. They utilized the method to model the flow of fluids in heterogeneous reservoirs, and produced a generalized model of the reservoir dynamics to deduce the interaction between injectors and producers. However, the method failed to account for sensitivities like fluid properties. With the lack of physical process representation in training, as well as the immense flexible outcome, the authors had suggested the limitations in this artificial neural network process.

Soeriawinata et al. (1999) also utilized Spearman rank, and further applied the superposition principle to production data in a typical five-spot pattern synthetic reservoir, from which they introduced the concept of constructive and destructive interference. They further tested the procedure observed from the synthetic case to a practical field. They stated that the cross correlations were lower between injector and producers because of the injected water flowing outside the lease boundary. They brought up the threshold for meaningful cumulative cross correlation, and from which they identified the strong connectivities and potential barriers. However, the selection of the threshold was arbitrary, as the authors admitted, and they eventually applied multiple different threshold numbers

due to the difficulty determining the threshold value. The other difficulty would be distinguishing the increase in cross correlation is due to superposition effect or the noise in the data. They suggested that the significant increase could be caused by constructive interference rather than the noise.

2.3 Model-based Tools for Inferring Interwell Connectivity

In 2002, Albertoni and Lake combines a multivariate linear regression with diffusivity filters to the injection and production data, in order to give information about the permeability trends and transmissibility barriers. The diffusivity filter accounts for the effect of the time lag and the attenuation between an injector and producer. And according to their observation, it improved the results and had wider range of application. They concluded that the connectivity between wells depends on coefficient that only on geology or relative position of the wells. The application of this technique requires assumptions that all the parameters in the field must be constant during the time period selected for analysis. The variables that need to remain unchanged through times are: well numbers, bottom-hole pressure, operating conditions, well productivity, gas-oil ratio. Also, the primary production accounted for the overall production should remain constant. Deviation from these assumptions would cause errors. The other error sources which worth noticing are: the data quality, open boundaries, and injector loses.

Based on Albertoni and Lake's work, Yousef (2005) proposed a more complete model that take the compressibility and transmissibility effects into account, which was named as capacitance-resistive model, to quantify the communication between vertical wells from the production and injection rates fluctuations. For each injector and producer pair, they determined two coefficients independent of the rates to infer the communication

between them. The weight quantifies the connectivity whereas the time constant quantifies the degree of the fluid storage between the wells. The new procedure resolved two constrains form the previous work: It can be applied to wells that contains shut-in period, and to fields that have remnant of primary production. Moreover, they incorporated the bottom hole pressure in to the model, to improve the results just from the rates performance.

Dinh and Tiab (2007) applied constrained multivariate linear regression using the fluctuation of bottom hole pressure of injectors and producers in waterflood reservoir to obtain the information to infer interwell connectivity and give information about the permeability trends and potential barriers. They observed better results compared to the same method previously with production data done by Albertoni and Lake. Nevertheless, they also resolved some limitations such as the use of diffusivity filter, the minimum data points needed, and data quality.

Sayapour et al. (2009) further developed Capacitance-Resistive Model, based on Yousef's (2005) model rooted in signal analysis and material balance using injector and producer's rate performance. By applying history matching process to the existing rates data, the method can utilize the production segment through any period of a field's life. It gives insights into the reservoir overall performance and also be able to predict future production. The pattern allocation factor tells the fractions of the injected water to each producer, whereas the time constant tells the time taken for the injector signals to travel to the corresponding producer. They provided analytical solutions for three different control drainage volume: the entire field, the single producer, and the volume between an injector and a producer.

2.4 Signal Processing Application in Oil and Gas Industry

Reservoir can be viewed as a complete system, while injecting and producing operations are the stimulus and response. The rate performance are signals that can be obtained and monitored easily as a tool to understand the reservoir behavior. Time lag and attenuation is accordingly the delay and dissipation for the signal to travel through the system due to the influence of porous media. Following these assumptions, researchers has been establishing methods applying signal-processing into oil and gas industry.

Hou et al (2012) introduced a signal convolver to preprocess injector's signal to account for its time lag and attenuation. According to their study, the production rates are treated as part or full response of injection rate, for unbalanced or balanced state respectively. They studied the influence factors of various reservoir parameters on the time lag and attenuations. They concluded that the injector-producer system of waterflooding reservoir is a first-order linear system. And they found relationships between time constant and porosity, pressure and well spacing.

4D seismic reservoir surveillance provides an opportunity to capture the acoustic contrast between reservoir fluids, enable us to monitor flood pattern around injector wells. The 4D signal was generated by subtracting the monitor seismic attributes by the baseline seismic surveys. The time-lapse seismic analysis based on 4D seismic interpretation can be used to qualitatively depict the movement of injected water. It can clarify the existence of channel between injector and producer, which answers the cause of the early water breakthrough which could not be getting from reservoir simulation (Danaei et al 2018).

Chapter 3: Digital Signal-Processing Method-based Indicators

I treat the injector-producer pair within a reservoir as a two-channel, digital transmitter-receiver system. For instance, water injection rates are input signals, while liquid production rates are output signals, as shown in Figure 1. These signals are, however, different from the conventional stationary time series, such as acoustic or electric signals. Notwithstanding, I borrowed the concepts from signal-processing literature and applied the analyses to oilfield data to quantify the degree or level of interwell connectivity. In this work, I examined cross-correlation, magnitude-squared coherence, covariance (periodicity), cross-power spectral density, bivariate histogram periodogram, and mutual information. I applied them to various well variable pairs and their derivative functions that will be discussed later.

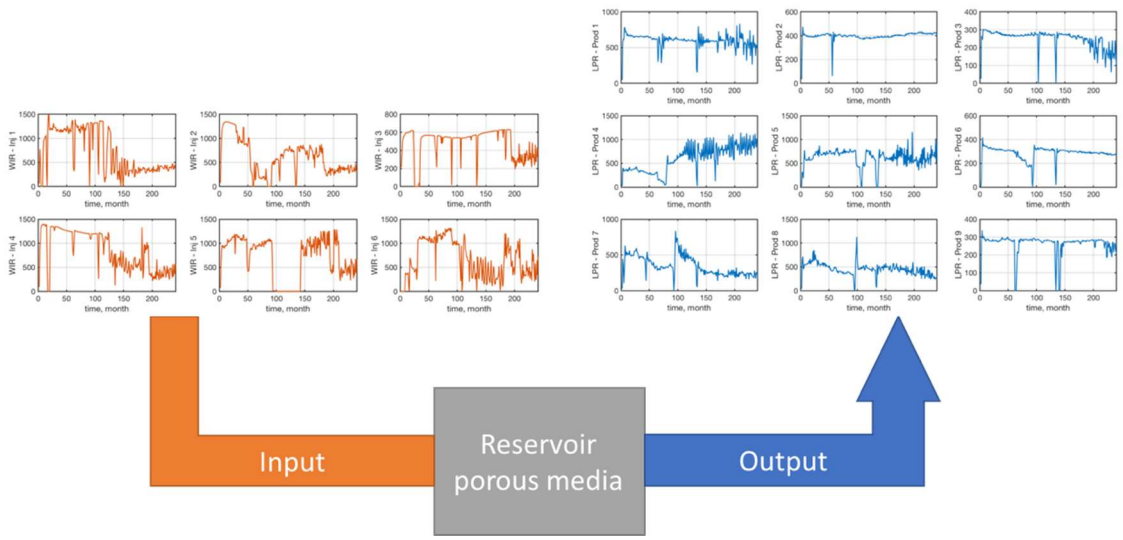

Figure 1. Schematic diagram of the injector data as input signals, production data as output signals, and reservoir porous media as a system.

I examined the information contained in the fluctuations of the well-based measurements and their derivative functions. I explored the similarity measures in injector-producer pairwise well variables to ascertain if they provide information relevant to

interwell communication. I followed a hierarchical approach starting with simple two-well scenarios under various reservoir conditions and then graduated into complex multi-well realistic reservoir framework undergoing waterflood. Having probed various similarity measures to be discussed later, I identified and proposed several rules of interwell connectivity indicators based on our hypotheses. These indicators are statistically compared with streamline-based injector-producer pairwise allocation factors (which I consider as the truth in realistic Design of Experiments (DoE) framework). Additionally, our indicators are compared against capacitance-resistance model (CRM)-based interwell connectivity measures.

This chapter will introduce the definitions and the applied concepts of three digital signal-processing techniques, which are: cross correlation, magnitude-squared coherence, and periodogram, among others. The algorithms based on these techniques applying injector and producer signals are presented, as well as the proposed indicators that I used to conduct later investigations.

3.1 Cross-correlation

Cross-correlation analysis determines similarity measures between two time-series (here, the injector signals and the producer signals) as a function of the lag or displacement of one signal for the other (Buck et al. 2002). The lag or time-shift can both be positive or negative, thus it can be presented in a two-sided manner. I will examine both the left lag and the right lag to infer connectivity information. Mathematically, cross-correlation, $R_{ip}(k,t)$, is equivalent to

$$R_{ip}(k) = E\{s_{t+k}^{i} s_{t}^{p^*}\} = E\{s_{t}^{i} s_{t-k}^{p}{}^*\} \quad (1)$$

where the asterisk stands for the complex conjugation, E is the expected value operator, s_t^i and s_t^p are the discrete-time injector and producer signals at time t and k is the lag in the time domain. The maximum of the cross-correlation function, if it is positively correlated, indicates the point in time lag where the signals are best aligned. Accordingly, the lag at this point is equal to the delay. As different variables have a significantly different range of values, I used normalized cross-correlation so that the autocorrelation[1] of each signal will have a value of 1 at zero lag. With normalization, the cross-correlation can be given as

$$\overline{R_{ip}}(k) = \frac{R_{ip}(k)}{\sqrt{E\{s_t^i s_t^{i^*}\} - E\{s_t^p s_t^{p^*}\}}} \tag{2}$$

Based on our extended definition of cross-correlation coefficient, and also the analysis using various synthetic simplistic two-well and complex multi-well realistic reservoir scenarios, I propose the following indicators to investigate interwell connectivity information (in brackets I itemize the corresponding labels that will be used henceforth):

1. Time lag at the first peak of cross-correlation coefficients of injector-producer well-variable pairs with negative shifts (XC1L)
2. The amplitude of the first peak of cross-correlation coefficients of injector-producer well-variable pairs with negative shifts (XC1A)
3. Time lag at the maximum peak of cross-correlation coefficients of injector-producer well-variable pairs with negative shifts (XC2L)

[1] Autocorrelation: the correlation of a signal with a delayed copy of itself, as a function of delay

4. The amplitude of the maximum peak of cross-correlation coefficients of injector-producer well-variable pairs with negative shifts (XC2A)
5. Time lag at the first peak of cross-correlation coefficients of injector-producer well-variable pairs with positive shifts (XC3L)
6. The amplitude of the first peak of cross-correlation coefficients of injector-producer well-variable pairs with positive shifts (XC3A)
7. Time lag at the maximum peak of cross-correlation coefficients of injector-producer well-variable pairs with positive shifts (XC4L)
8. The amplitude of the maximum peak of cross-correlation coefficients with positive shifts (XC4A)

Figure 2 illustrates these items. Note I measure the lags from the zero-offset along the x-axis and the amplitudes from the zero-offset along the y-axis as depicted in Figure 2.

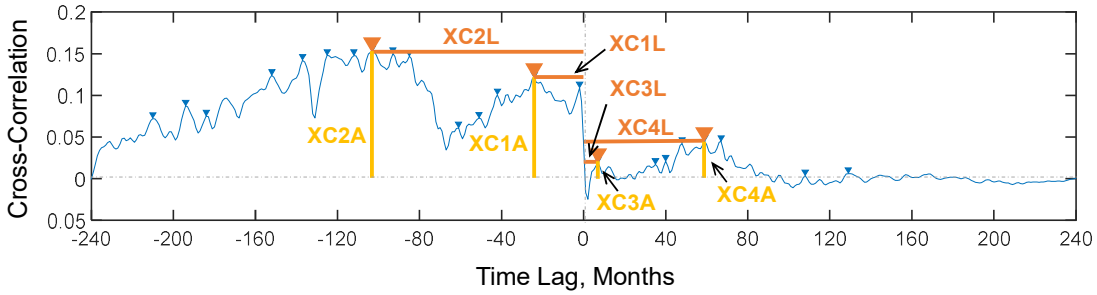

Figure 2. Cross-correlation coefficient profile of a well-variable pair showing both negative (left side) and positive (right side) time-shifts. Connectivity indicators based on cross-correlation coefficients are pointed out in the figure.

3.2 Magnitude-Squared Coherence

Spectral analysis is another broad class of common parametric data analysis approaches for time-series data. This tool provides means to parameterize the spectrum and

thereby reduces the spectral estimation problem to that of evaluating parameters of the assumed model (Stoica and Moses 2004). In this study, I will only use magnitude-squared coherence and periodogram.

Magnitude-Squared Coherence (MSC) enables us to identify the dominant frequency content of two time-series (Trauth 2006). Like cross-correlation, it is a measure of correlation or similarity however in frequency domain. The time-series data are converted to frequency spectrals by Discrete Fourier Transform (FFT). MSC values range between 0 and 1. These values indicate how well one signal corresponds to another at each frequency. The magnitude-squared coherence is a function of the power spectral densities, $PSD_{ii}(f)$ and $PSD_{pp}(f)$, and the cross power spectral density, $PSD_{ip}(f)$, of the two signals in frequency domain s_f^i and s_f^p at the frequency f:

$$C_{ip}(f) = \frac{\left|PSD_{ip}(f)\right|^2}{PSD_{ii}(f)PSD_{pp}(f)} \tag{3}$$

The Magnitude-Squared Coherence (MSC) based indicators are as follows (in brackets I itemize the corresponding labels that will be used henceforth):

1. Eigen-frequency or the most dominant frequency of injector-producer well-variable pairs in MSC (MSC1)
2. The maximum magnitude of injector-producer well-variable pairs in MSC (MSC2)

Figure 3 gives an example of these indicators based on magnitude-squared coherence profile of one injector and one producer signals.

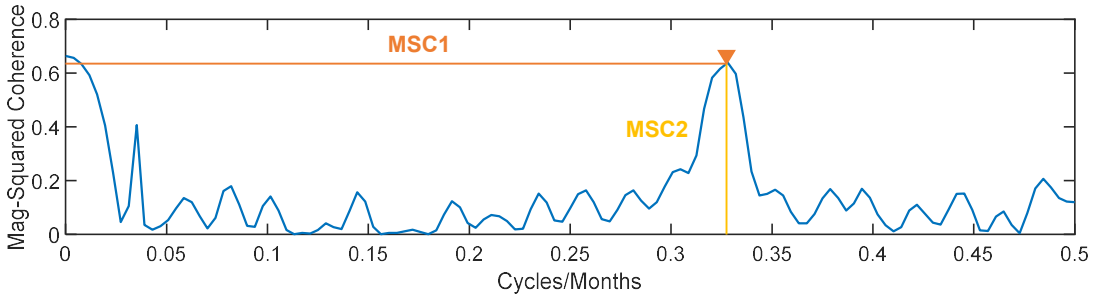

Figure 3. Magnitude-squared coherence profile of a well-variable pair showing the connectivity indicators.

3.3 Periodogram

Periodogram is a nonparametric estimate of the power spectral density (PSD) of a frequency domain signal (Stoica and Moses 2005). It focuses on the features of one signal by itself. It has found wide usage in examining the frequency characteristics of noise-free functions, such as filter impulse responses and window functions. Periodogram can be expressed as

$$\widehat{Per}(f) = \frac{\Delta t}{N}\left|\sum_{t=0}^{N-1} s_t^{\alpha} e^{-i2\pi ft}\right|^2 \tag{4}$$

where N is the number of data, s_t^{α} is a signal from the time series at time t, f is the frequency, i the imaginary number, while the superscript α denotes injector or producer.

Periodogram-based indicators are as follows (in brackets I itemize the corresponding labels that will be used henceforth):

1. The difference in the maximum power spectral density of signals from injector and producer in the periodogram (PSD1)
2. The difference in the frequency where the maximum power occurs in the signals from injector and producer in the periodogram (PSD2)

Figure 4 identifies these indicators. Because periodogram focuses on the feature of one signal by itself, the example shows two spectrums, with one from the producer in blue, and one from the injector shown in red.

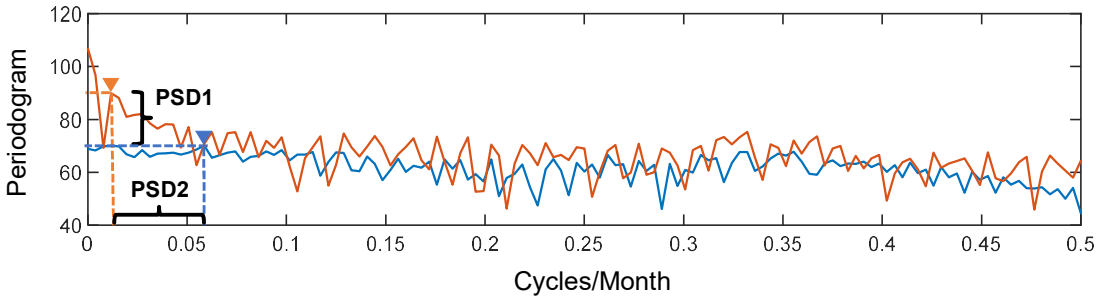

Figure 4. Periodogram profiles of a well-variable pair showing the connectivity indicators.

The signal-processing methods I utilized provide reasonably high-resolution estimators for large data sets but can have poor spectral estimators because of high variance. I explored several smoothing methods to reduce the variance at the cost of reduced resolution. This step yielded improved and more prominent parametric results. In all the cases presented in this work, I applied a smoothing method named "locally weighted scatterplot smooth" or in short "lowess". This approach is similar to the moving-average method where each value is determined by neighboring data points defined within a span[2]. After that, I apply a regression-weight function.

3.4 Well-variable Pairs

In this study, I examined many well variables and derivative functions to exploit the information content relevant to interwell communication. In all cases, I need a signal or variable from an injector and another from a producer and determine their similarity or

[2] Span: a percentage of the total number of data points, less than or equal to 1.

dissimilarity measures. These data coming from the wells need certain degree of fluctuations in order to proceed with signal-processing techniques. Although I have explored many combinations of well-variable pairs, not all the pairs could be proved informative. In this thesis, I selected a subset of them based on the representative level of their profiles, and presented them in the same order for different digital signal-processing techniques. The variable-pairs are injector and producer bottom-hole pressure (BHP); water-injection rates – production rates (examined oil rates, water rates, liquid rates, and reservoir volume rates); injector productivity index (PI) – producer PI; injector well variables (BHP, PI or water injection rates) – producer gas-oil ratio and watercut; and a pair $F1 - F2$, of derivative functions of well-variables. Table 1 shows the abbreviation of these variables, as well as the descriptions of the abbreviations that will appear in the figures in the following chapters.

Well Variables	Descriptions
WPR	Water Production Rate, STB/day
LPR	Liquid Production Rate, STB/day
OPR	Oil Production Rate, STB/day
RVPR	Reservoir Volume Production Rate, bbl/day
BHP	Bottom Hole Pressure, psia
WC	Water Cut
GOR	Gas-oil Ratio, SCF/STB
WIR	Water Injection Rate, STB/day
PI	Productivity Index

Table 1. Listed well variables and descriptions.

Upon examination, I found $F1 - F2$ to be one of most informative well-variable. The definition of $F1$ and $F2$ are provided in the equations below.

$$F1 = \frac{\mathrm{d}q(t)}{\mathrm{d}t} + J\frac{\mathrm{d}p_{wf}(t)}{\mathrm{d}t} \tag{5}$$

$$F2 = i(t) - q(t). \tag{6}$$

Here, $q(t)$ is the production rate, as discussed above the rates examined can be water, oil, liquid and reservoir volume production rate in the analysis; whereas $i(t)$ is the injection rate, p_{wf} is the bottom-hole pressure of the producer, and J is the producer productivity index. $F1$ is nothing but the decline in production rate that accounts for pressure depletion as well. $F2$ is the difference in the rates for the producer and the injector. At any instance, $F2$ provides relative withdrawal of fluids from the system. $F1$ and $F2$ have both underpinnings in material-balance of the system (Sayarpour, 2008). Incidentally, the ratio of $F2$ and $F1$ has units of time. Herein, we are using the extended meaning of these variables. Another characteristic of the derivative functions is that these functions can amplify the signals (as well as the noise). As an exploratory work, I try to pursue if these variables can give us more connectivity information through a systematic examination.

In the following chapters, I will describe the applications of the proposed connectivity indicators under various reservoir conditions.

Chapter 4: Simple Two-well Scenarios

I took a systematic and hierarchical approach to examining the well-variable pairs with the connectivity indicators described in Chapter 3. In this chapter, I will discuss the investigations of signal-processing methods and proposed indicators by simplistic two-well scenarios.

I will start with introducing the reservoir model construction, and then move on to examining the signal-processing techniques: cross-correlation coefficient, magnitude-squared coherence, and periodogram under various conditions, including: well distance effect, layer-wise zonation effect, well interference effect and heterogeneity effect. From these investigations, I am going to decide the most informative well-variable pairs, and carry it on to more complex multi-well scenarios.

4.1 Reservoir Model Construction for Two-well Scenarios

For the two-well scenarios, I considered geological models with four zones (upper, middle, lower and bottom zones). The top of the structure is at a depth of 5,100 ft and the bottom of the structure at 5,300 ft. The model included 114,800 cells (144×150×53) in a 7,200 ft × 7,500 ft grid. Figure 5 displays the model schematic. As the simplest case (base case), I kept the petrophysical properties homogeneous and same for all the zones. Table 2 presents the rock and fluid properties used in the simulations. The static properties are determined by using the median values from a statistical study based on numerous of conventional wateflood projects in the Permian basin of West Texas and southeast New Mexico (Ordonez et al, 2018). The injector and producer are about 1,250 ft apart in the base case.

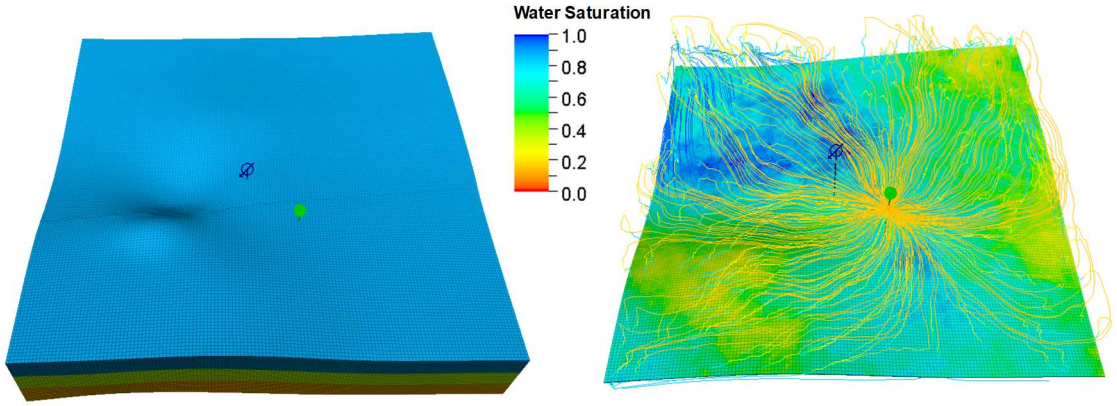

Figure 5. Schematic of the simple two-well reservoir cases. (a) 3D model displaying the 4 zones (upper, middle, lower and the bottom) and the injector and the producer, (b) streamlines with water saturation.

Horizontal permeability (md)	15.5
Vertical permeability (md)	1.5
Porosity (%)	13
Water-oil contact depth (ft)	5,265
Oil density (°API)	35
Gas specific gravity	0.65
Water salinity (ppm)	70,000
Solution GOR (Mscf/STB)	0.50
Residual oil saturation	0.30
Critical water saturation	0.20
Water saturation at P_c=0	0.55
Capillary pressure at water-oil contact (psi)	2.00
Rock compressibility (psi^{-1})	1.30E-05

Table 2. Some static properties for the base geological model.

I performed streamline simulations using a commercial simulator (Schlumberger 2016) for 20 years (240 months) using rate controls (the injector using surface water injection rate and the producer using oil production rate) and bottom-hole pressure limits. The minimum production bottom-hole pressure limit is 250 psi, and maximum injection bottom hole pressure limit is 3,900 psi[3]. The reporting frequency is once a month, and that gives us the 240 data points for every case.

[3] The bottom-hole pressure was limited to 3,900 psi so that the pressure gradient does not reach the fracture gradient (typically around 0.8 psi/ft or more).

4.2 Examination of Signal Processing Techniques with Well Distance Effect

To capture the effect of distance between the injector and the producer, I halved and doubled the distance in the base case. The schematic relative position of these wells are shown in Figure 6. Figure 7 presents the well variables obtained from these three cases. Variables include (listed in order displayed) water production rate (WPR), liquid production rate (LPR), oil production rate (OPR) in STB/day, gas-oil ratio (GOR) in SCF/STB, bottom-hole pressure of producer (Prod BHP) in psia, water cut, water injection rate (WIR), bottom-hole pressure of injector (Inj BHP) in psia and reservoir volume production rate (RVPR) in bbl/day.

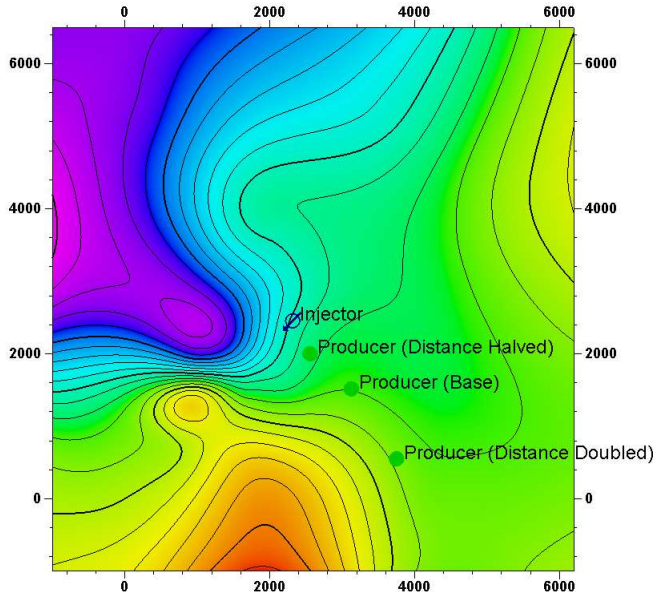

Figure 6. Schematic of relative distance between injector and producer in the two-well scenarios with well distance effect. The contours in the background are based on the elevation of the top surface.

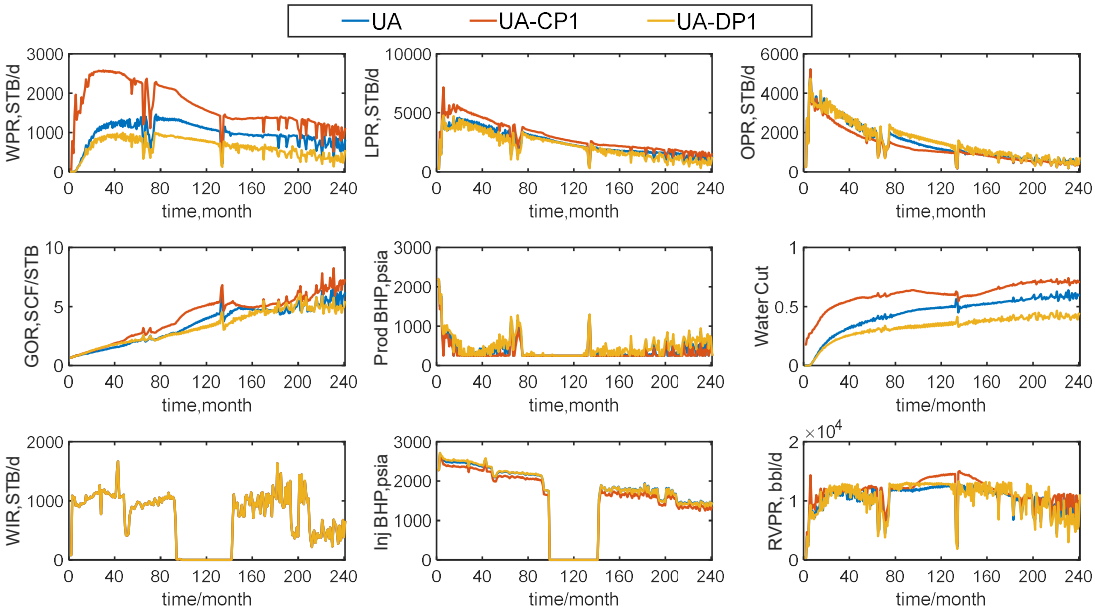

Figure 7. Simulated well variables for the homogenous cases with well distance effect.

The case labels as follows: Blue line is the base case (UA), red line is the case with closer well distance (UA-CP1), and yellow line is the case with distant well distance (UA-DP1). With distance halved the most prominent effect appears to be in the water-production rates. I observe the water production rate has increased (in UA-CP1) and the distance doubled it reduced (in UA-DP1). Watercut profiles show similar strong variation. I see a corresponding but somewhat muted effect in oil, liquid, and reservoir-volume production rates. The bottom-hole pressure variation gets much muted given the simulation is in rate-control mode. The injector contains a shut-in period for about 10 months, but the production doesn't get affected a lot, indicating the primary production still contributes a large portion in this production activity.

Using these well variables and the three cases illuminating the distance effect, I obtained the cross-correlation coefficients for various injector-producer well-variable pairs. For brevity, Figure 8 displays only 12 well-variable pairs. These pairs include (list

in order) producer bottom-hole pressure (BHP) – injector BHP, gas-oil ratio (GOR) – injector BHP, GOR – water injection rate (WIR), GOR – injector productivity index (PI), water production rate (WPR) – WIR, liquid production rate (LPR) – WIR, oil production rate (OPR) – WIR, reservoir-volume production rate (RVPR) – reservoir-volume injection rate (RVIR), watercut (WC) – WIR, injector PI – producer PI, $F1-F2$ using LPR and $F1-F2$ using RVPR. The three colors represent the effect of different well distances on these digital signal-processing techniques. Blue line is the base case (UA), red line is the case with closer well distance (UA-CP1), and yellow line is the case with distant well distance (UA-DP1). From the cross-correlation profiles, I can see clearly the $F1-F2$ variable pairs contain more noticeable fluctuations and differences with the distance effect. Other variable pairs like GOR – Injection PI and Producer PI – Injector PI also shows informative, but weather if they have consistent performance will be determined by further investigation of more cases.

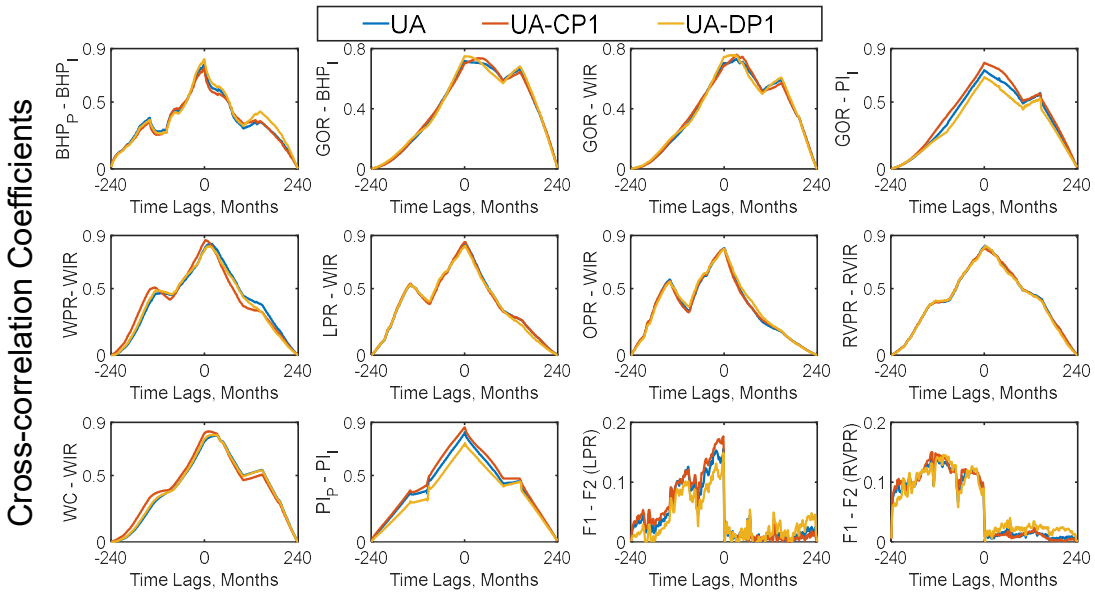

Figure 8. Cross-correlation coefficients of various injector-producer well-variable pairs for the homogenous cases with well distance effect.

Figure 9 shows the corresponding magnitude-squared coherence (MSC) profiles for the same well-variable pairs and the three cases. Figure 10 illustrates the periodogram profiles for the same well-variable pairs but only for the base case. As periodogram profiles require one time-series signal at once and I compare the similarity measures of two time-series by examining the differences in the power spectral densities and the corresponding frequencies, I displayed only the base case. Note, in these three figures (Figure 8, Figure 9, and Figure 10), I deliberately avoided showing the connectivity indicators to prevent clutter.

The magnitude-squared coherence profiles shows a noteworthy distinction in the variable pair BHP – BHP, GOR – WIR, GOR – PI, WPR – WIR, and $F1 - F2$ pairs. For periodogram, as it is hard to compare the effect between different cases, I will not further address the analyses based on periodograms henceforth in this thesis. However, the information shown in the periodogram profiles could provide ideas for future study.

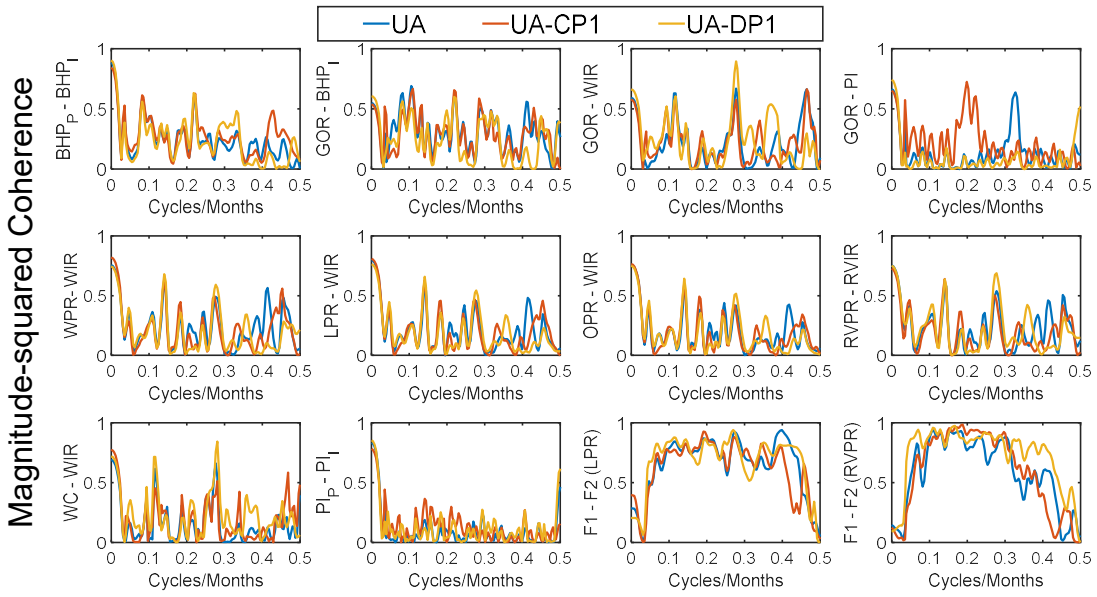

Figure 9. Magnitude-squared coherence of various injector-producer well-variable pairs for the homogenous cases with well distance effect.

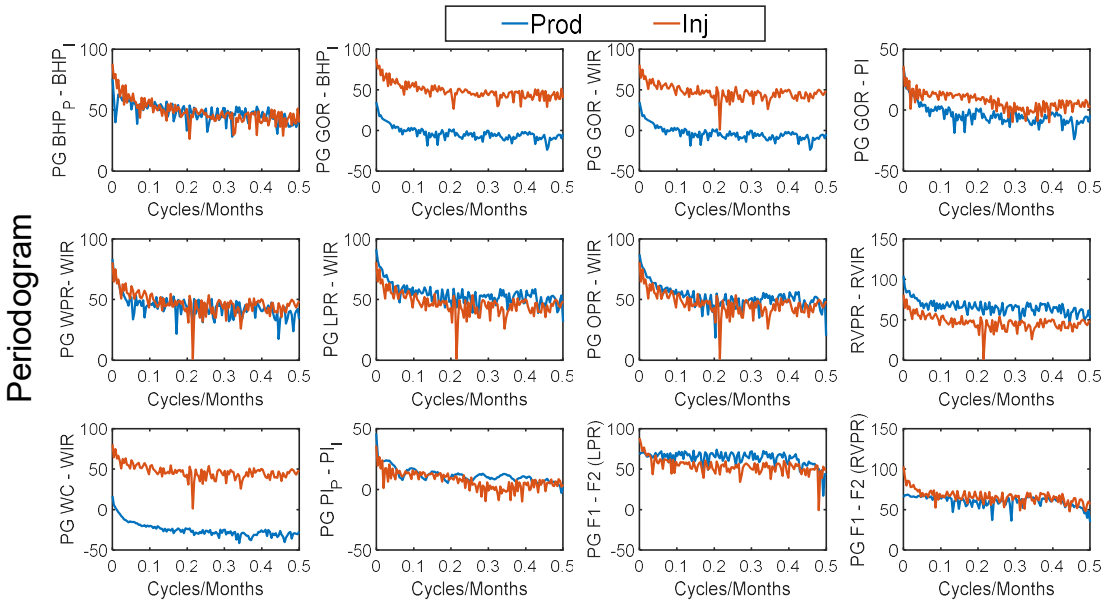

Figure 10. Periodogram profiles of various injector-producer well-variable pairs for the homogenous cases with well distance effect.

4.3 Examination of Signal Processing Techniques with Layer-wise Zonation Effect

Having observed the distance effect, I next investigate the effect of the layer-wise variation in porosity and permeability in comparison with the homogeneous case. In the layer-wise variation case, the porosity and permeability of the upper, middle, lower and bottom zones are shown in Table 3. The four layers represent the zone with high permeability, very low permeability (represents shale zone; the value is averaged from the statistics study of waterflooding projects in Permian basin, provided by Ordonez et al, 2018), intermediate permeability and moderate permeability. Figure 11 presents the well data in the same order as the previous case with well distance effect.

Case/Layer	Porosity	Horizontal permeability (md)	Vertical permeability (md)
UA (Homogeneous)	0.13	15.65	1.5
UL EA-EB (Upper zone)	0.14	27	2.7
UL EB-EC (Middle zone)	0.07	2.1	0.2
UL EC-ED (Lower zone)	0.12	6.3	0.6
UL ED-EE (Bottom zone)	0.12	5.7	0.5

Table 3. Porosity and permeability of each zone for the case with layer-wise zonation effect.

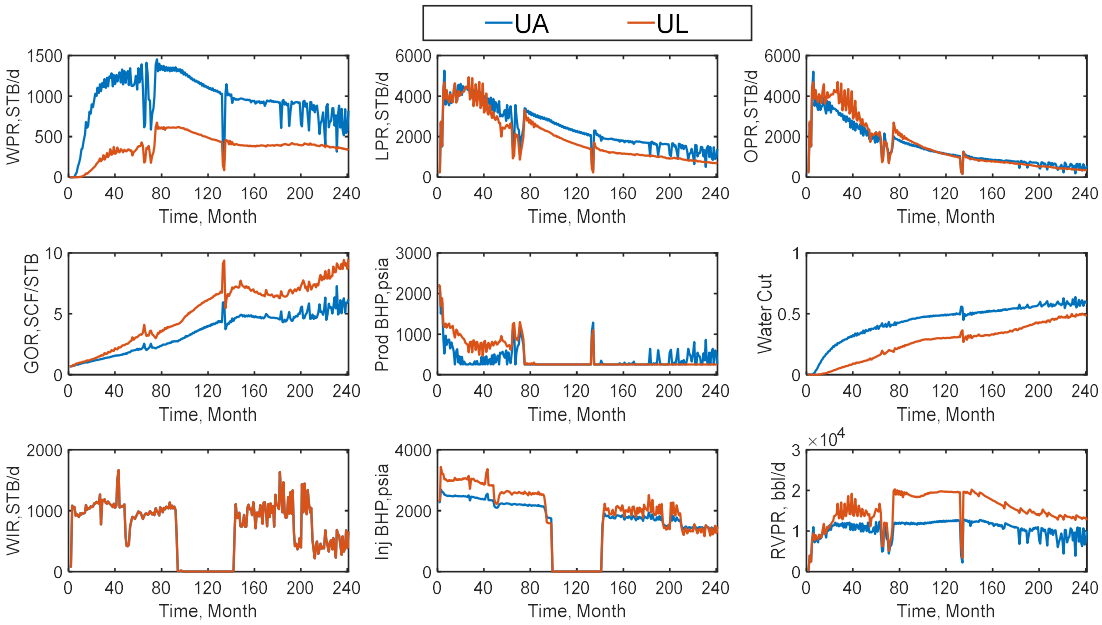

Figure 11. Simulated well variables for the cases with layer-wise zonation effect.

The case labels are as follows: Blue line is the base case (UA), red line is the case with layer-wise zonation effect (UL). For the layer effect, the most prominent signals appear to be, again, in the water-production rates. I observe the water production rate has decreased (in UL). Watercut profiles show similar strong variability. The GOR and reservoir-volume production rates are significantly higher. This is due to the effect of the low permeability zone in the middle that served as a barrier preventing vertical water movement. And the completion of the injector is also within the lower zones, at the depth around the water-oil contact. The schematic of completions and zone divisions are shown in Figure 12. The blue zone on the top is the most permeable zone, where the most oil production is coming from; the thin green zone in the middle is the shale zone; the bottom two zones, as shown in color yellow and orange, are the moderate permeable zone. For this same reason, we can see the bottom-hole pressure of the producer is noticeably greater (in UL), and accordingly the injector's bottom-hole pressure is higher as well. From these

observations, we can say that the reservoir energy is higher for production in this case, but with the primary production provides the support, if the connectivity of injector and producer in this case is better or not still need further discussion.

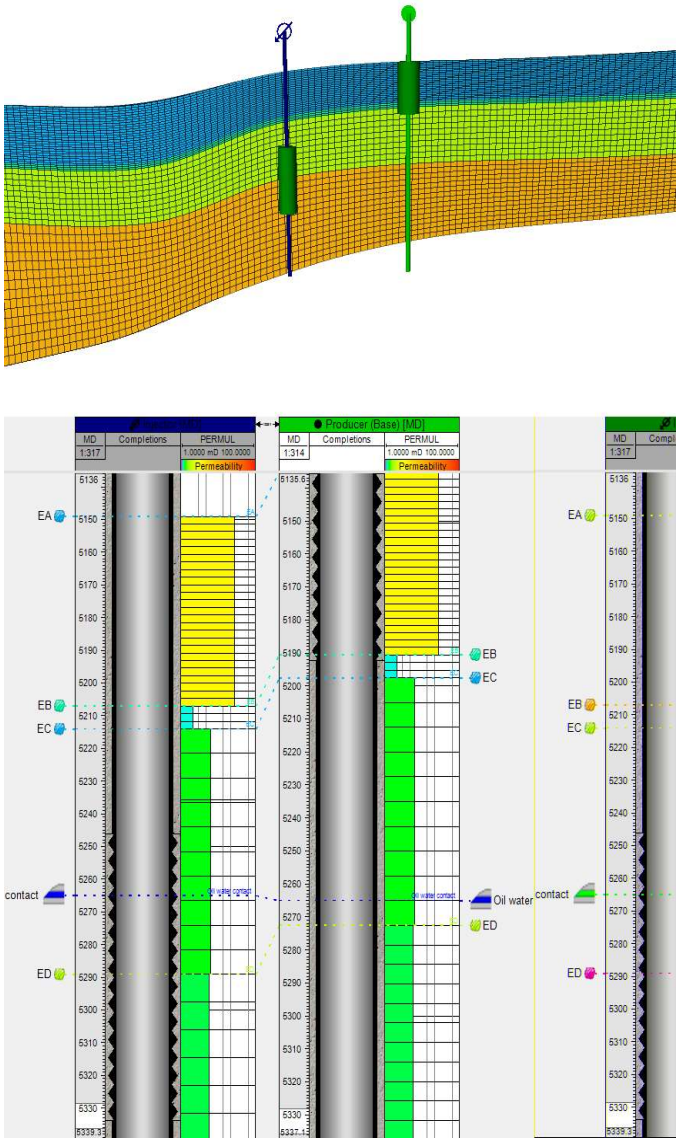

Figure 12. Schematic of model zone divisions and well completions.

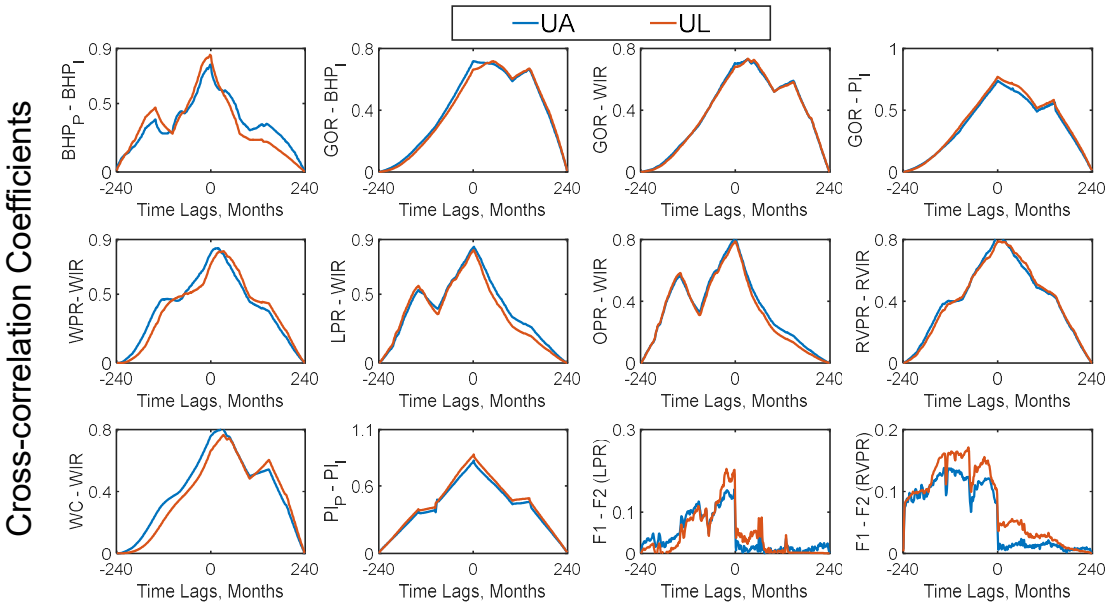

Figure 13. Cross-correlation coefficients of various injector-producer well-variable pairs for the cases with layer-wise zonation effect.

Using these well variables and the three cases illuminating the layer-wise zonation effect, I obtained the cross-correlation coefficients for various injector-producer well-variable pairs, as shown in Figure 13. For the sake of consistency, the profiles display the same 12 well-variable pairs with the previous investigation for well distance effect. The two colors represent the effect of zonation on these digital signal-processing techniques. Blue line is the homogeneous base case (UA), red line is layer-wise uniform case (UL). We are able to see the variation of the cross-correlation profile caused by layer effect from BHP – BHP, WPR – WIR, WC – WIR, and $F1 - F2$ pairs.

The magnitude-square coherence profiles are shown in Figure 14. All the variable pairs seem to contain significant variations due to the effect of different properties in the added zones. The most noticeable ones are: BHP – BHP, GOR – BHP, GOR – WIR, GOR – PI, WPR – WIR, RVPR – RVIR, and $F1 - F2$ pairs.

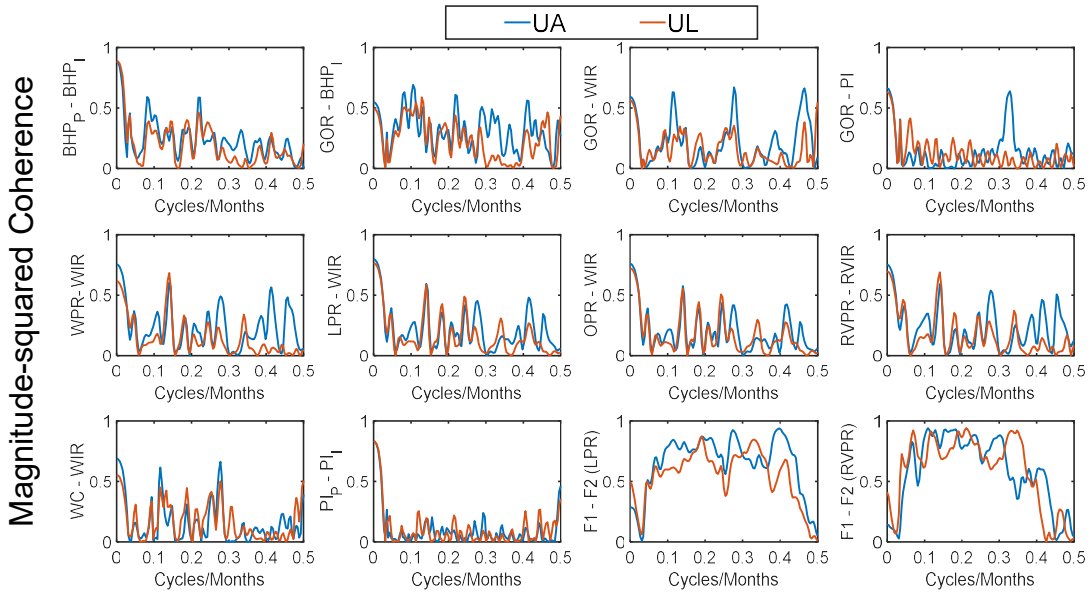

Figure 14. Magnitude-square coherence coefficients of various injector-producer well-variable pairs for the cases with layer-wise zonation effect.

4.4 Examination of Signal Processing Techniques with Well Interference Effect

I examined well interference effect by introducing another producer in the homogeneous case. With the other producer in place, I expect once the communication between the injector and the second producer establishes, the original producer will have less support from the injector. In order to keep the effect of other factors, e.g., geological influence, distance influence, etc. to a minimum extend, I select the producer which is located in a similar distance with the injector. Figure 15 shows schematic of the relative location of the injector, the original producer and the competing producer. The lines in color showed in the figure are the streamlines representing different source of fluid and energy. They help us to identify the starting and ending of fluid flow dynamically.

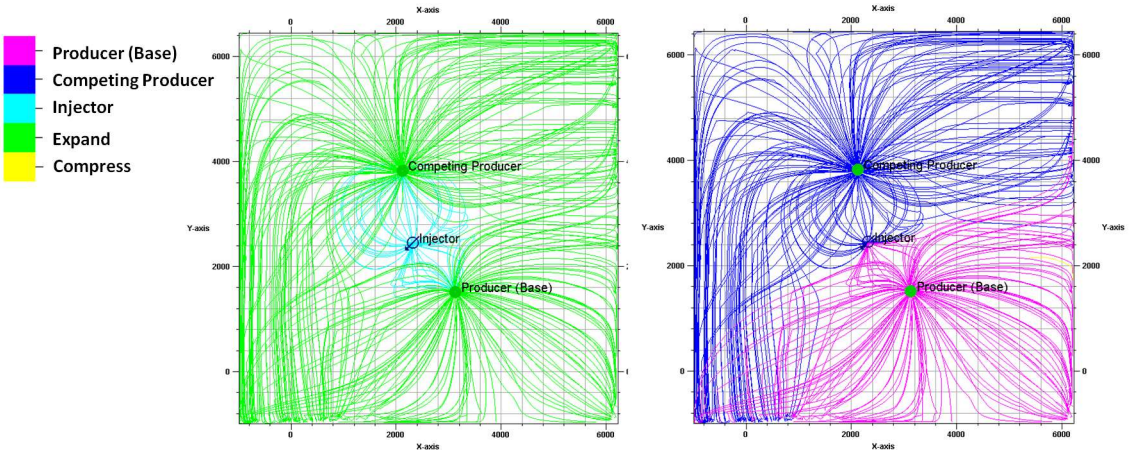

Figure 15. Relative geological location between the added competing producer and the original producer is within a similar distance.

It is also worth noticing here that streamlines connected to the producers do not just emanate from the injector alone. Figure 16 shows an example of the streamline fraction at the end of the simulation time step. We can see clearly that the injector only connects a small portion of the streamlines to the two injector. The majority of the production still comes from the natural drives in the reservoir. These streamlines represent expansion energy in the reservoir contributing to the majority fraction of the connected streamlines.

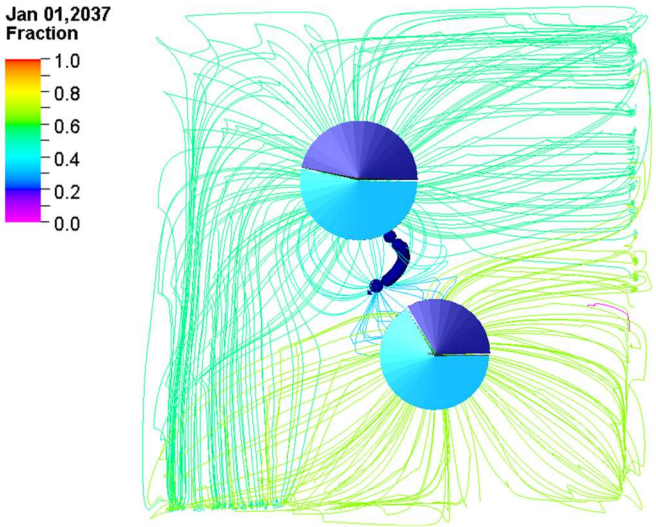

Figure 16. Example of streamline fraction at the end time step of simulation for two-well scenarios.

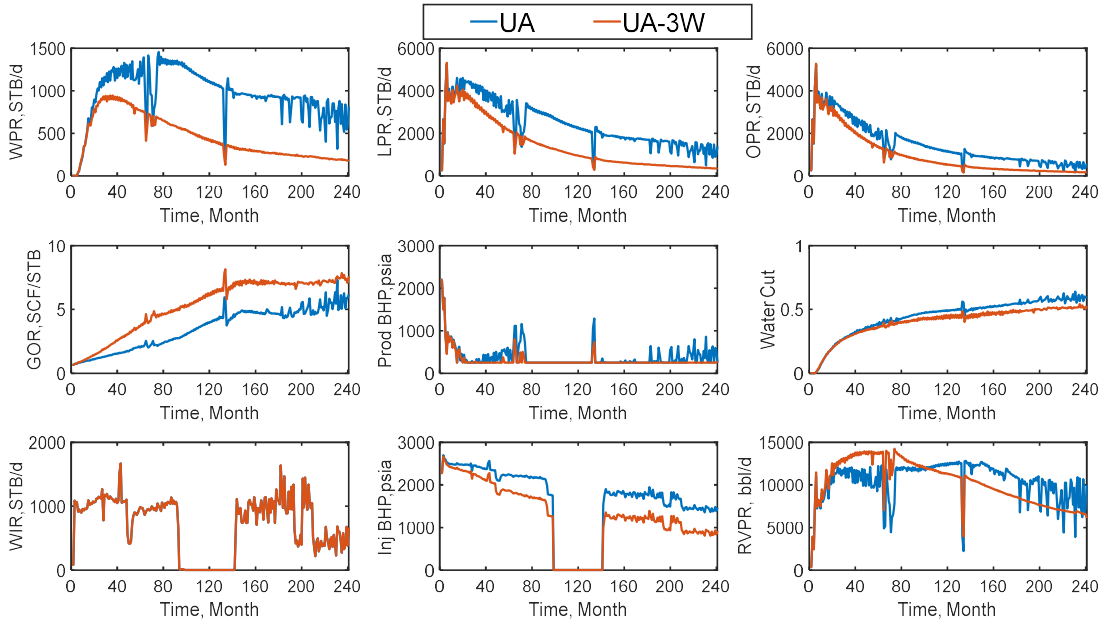

Figure 17. Simulated well variables for the cases with well interference effect.

The case labels as follows: Blue line is the base case (UA), which contains only one injector and producer; red line is the case with well interference effect (UA-3W), which contains one injector at the same geological position and two producers. With another well presenting, I can observe a prominent decrease in most of the production rates (in UA-3W). The GOR profile, however, are showing an opposite increase. The producer's bottom hole pressure hit the limit pretty fast, and remains little variation till the end of the simulation period, indicating the competing producer is actively consuming the energy provided to the base producer. For this same reason, I can see accordingly the injector's bottom-hole pressure is lower. Reservoir volume production rates are higher in the beginning, but then dropped gradually till the end.

Using these well variables and the two cases illuminating the well interference effect, I obtained the cross-correlation coefficients for various injector-producer well-variable pairs again, as shown in Figure 18. The profiles display the same 12 well-variable

pairs with the previous investigations. The two colors represent the effect of well interference on these digital signal-processing techniques. Blue line is the base case with one producer (UA), red line the case added another producer (UA-3W). We are able to see the variation of the cross-correlation profile caused by layer effect from WPR – WIR, LPR – WIR, OPR – WIR, and $F1 - F2$ pairs.

Figure 19 shows the magnitude-square coherence profiles. The most noticeable variable pairs that contain significant variations are: GOR – WIR, GOR – PI, WPR – WIR, RVPR – RVIR, and $F1 - F2$ pairs. It is worth noticing that till now $F1 - F2$ pairs present consistently informative variations with the effects.

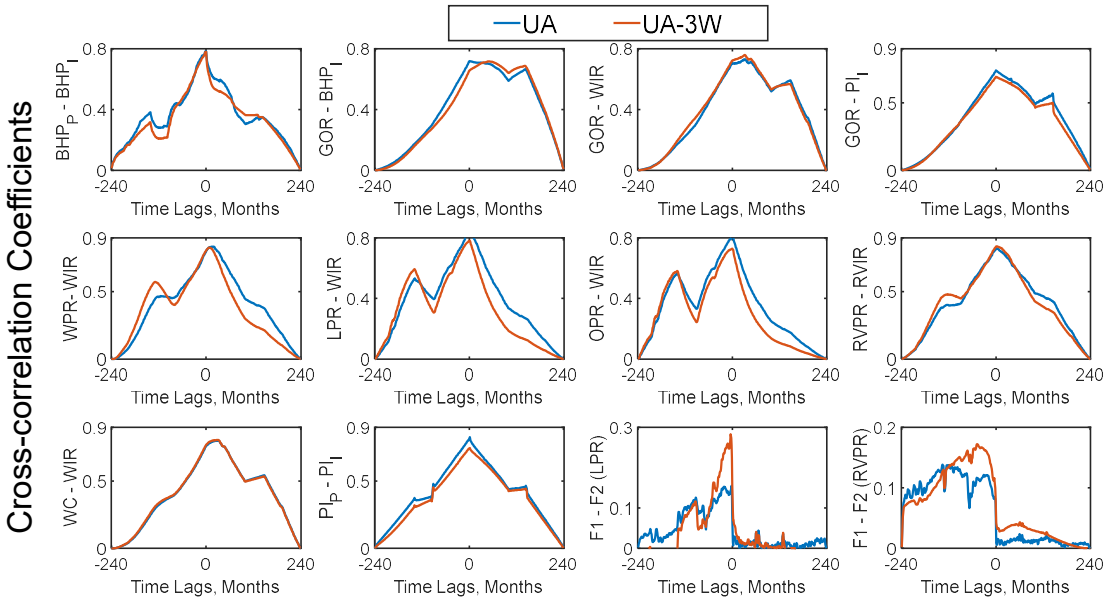

Figure 18. Cross-correlation coefficients of various injector-producer well-variable pairs for the cases with well interference effect.

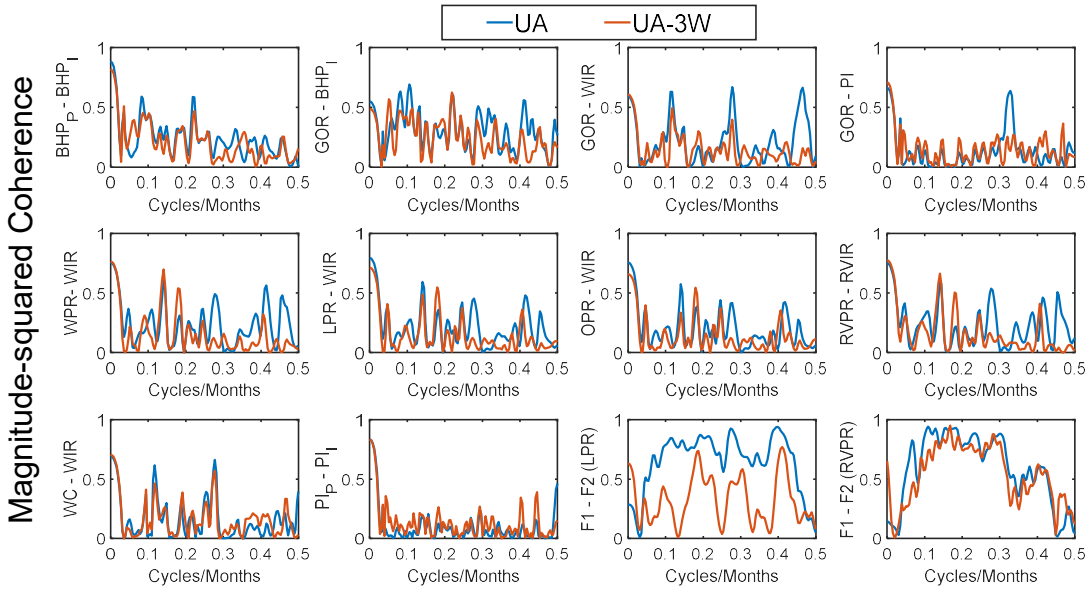

Figure 19. Magnitude-squared coherence of various injector-producer well-variable pairs for the cases with well interference effect.

4.5 Examination of Signal Processing Techniques with Heterogeneity Effect

To examine the effect of heterogeneity in porosity and permeability distribution, I constructed a simple heterogeneous reservoir model. The petrophysical models use Sequential Gaussian simulation for porosity and permeability models. The variogram inputs are shown in Table 4. The variogram type is spherical, and the nugget value is 0.0001. The porosity model follows a normal distribution, whereas the permeability model follows a lognormal distribution, with the minimum, maximum and mean data range shown in Table 5. The distribution profiles of porosity and permeability data for all four zones are shown in Figure 20. Figure 21 shows the well data from these two cases. The blue line is the homogenous base case, and the red line is the heterogeneity case as comparison.

Case/Layer	Anisotropy range			Orientation	
	Major	Minor	Vertical	Azimuth	Dip
UH EA-EB (Upper zone)	550	412.5	40	-30	0
UH EB-EC (Middle zone)	2000	1900	3	0	0
UH EC-ED (Lower zone)	400	240	7	15	0
UH ED-EE (Bottom zone)	3611	3611	17.2	0	0

Table 4. Variogram inputs for petrophysical modeling.

Case/Layer	Porosity			Permeability (md)		
	Min	Max	Mean	Min	Max	Mean
UH EA-EB (Upper zone)	0.025	0.25	0.137	0.5	100	30
UH EB-EC (Middle zone)	0.015	0.14	0.078	0.1	10	6
UH EC-ED (Lower zone)	0.02	0.23	0.125	0.25	80	7.5
UH ED-EE (Bottom zone)	0.02	0.23	0.125	0.25	75	5.6

Table 5. Petrophysical modeling parameter inputs for heterogeneous case.

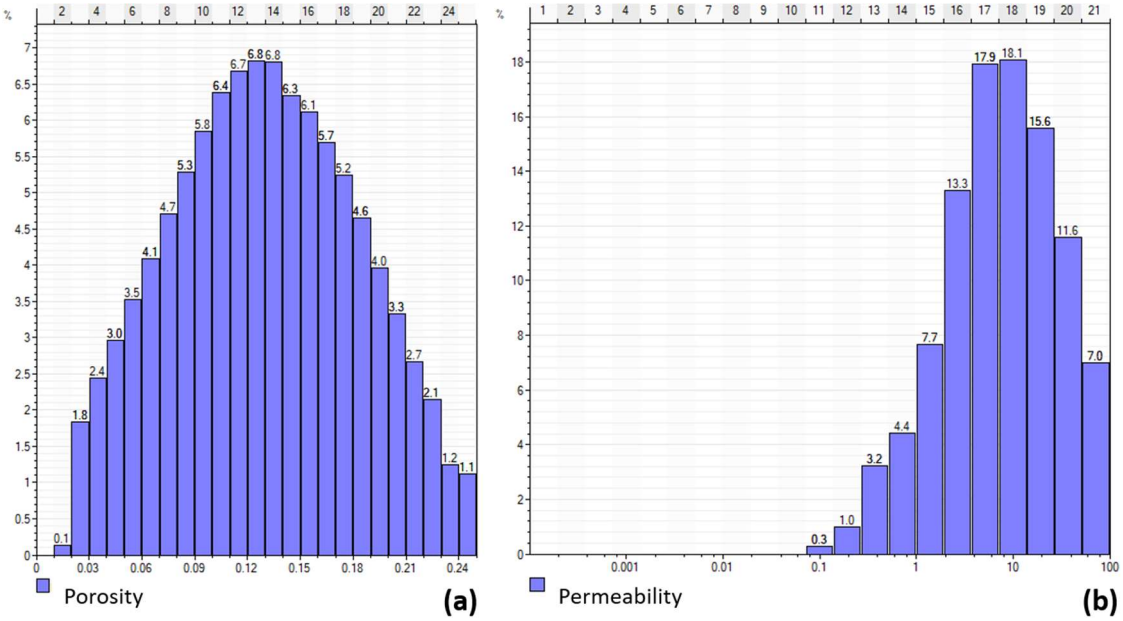

Figure 20. Distribution profiles for (a) porosity and (b) permeability model.

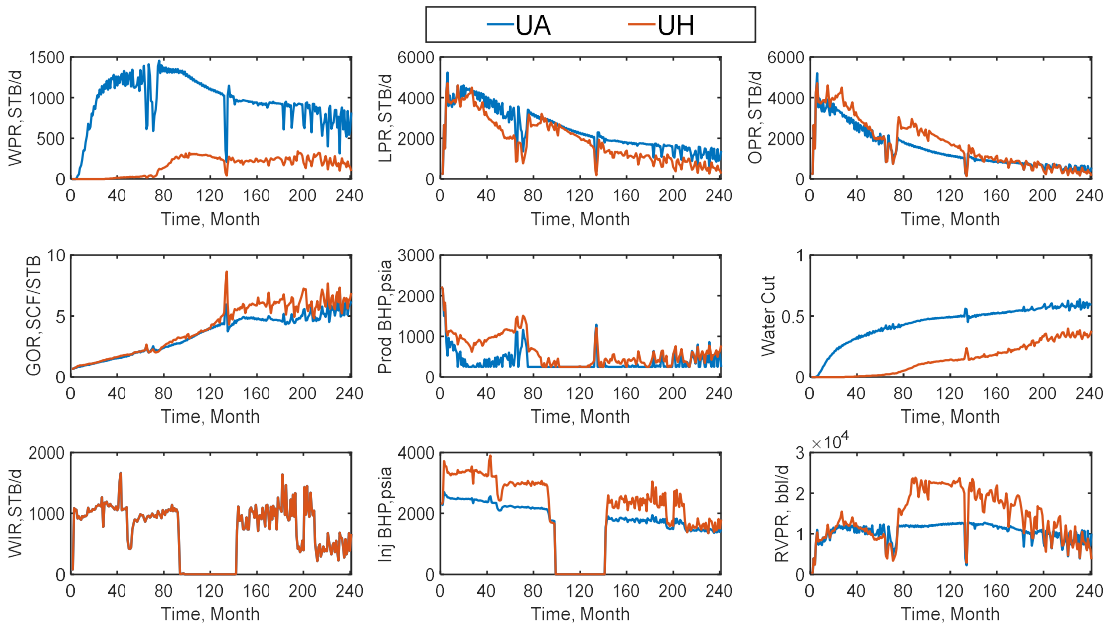

Figure 21. Simulated well variables for the cases with heterogeneity effect

From the well data, it is obvious that with the presence of heterogeneity, the water production as well as water cut decreased enormously. The production seems better at the later period after the water breakthrough, judged by the liquid, oil and reservoir volume production rate.

Using these well variables and the two cases illuminating the heterogeneity effect, I obtained the cross-correlation coefficients for various injector-producer well-variable pairs again, as shown in Figure 22. The profiles display the same 12 well-variable pairs with the previous investigations. The two colors represent the effect of heterogeneity on these digital signal-processing techniques. Blue line is the base homogenous case (UA), red line the heterogeneity case (UH). We are able to see the variation of the cross-correlation profile caused by layer effect from BHP – BHP, WPR – WIR, WC – WIR, and $F1 - F2$ pairs.

The magnitude-square coherence profiles are shown in Figure 23. All the variable pairs seem to have prominent variance. $F1 - F2$ pairs present consistently informative variations with the effects.

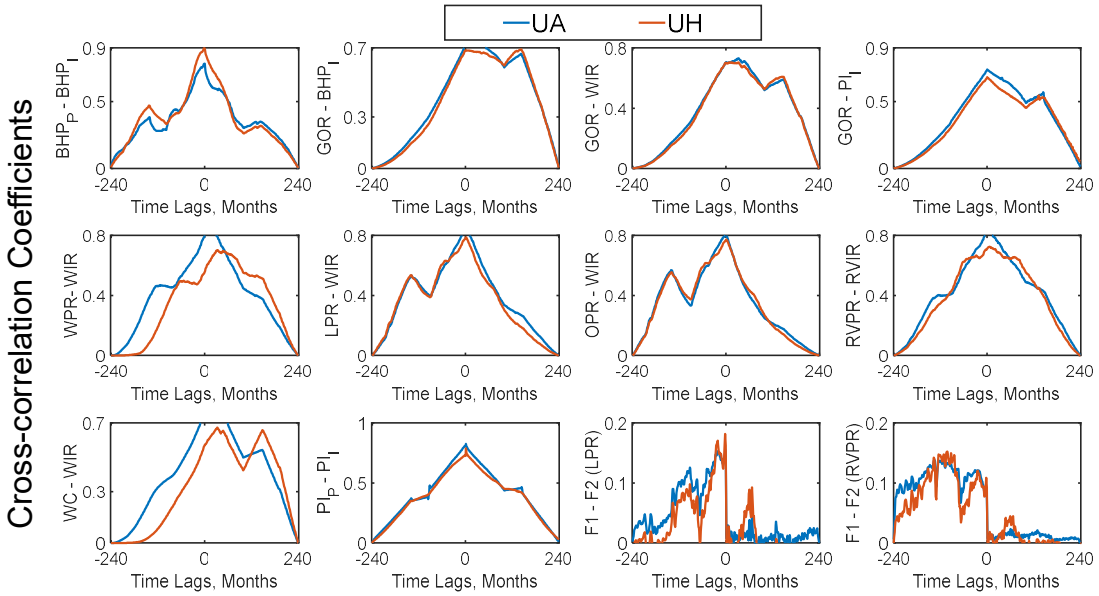

Figure 22. Cross-correlation coefficients of various injector-producer well-variable pairs for the cases with heterogeneity effect.

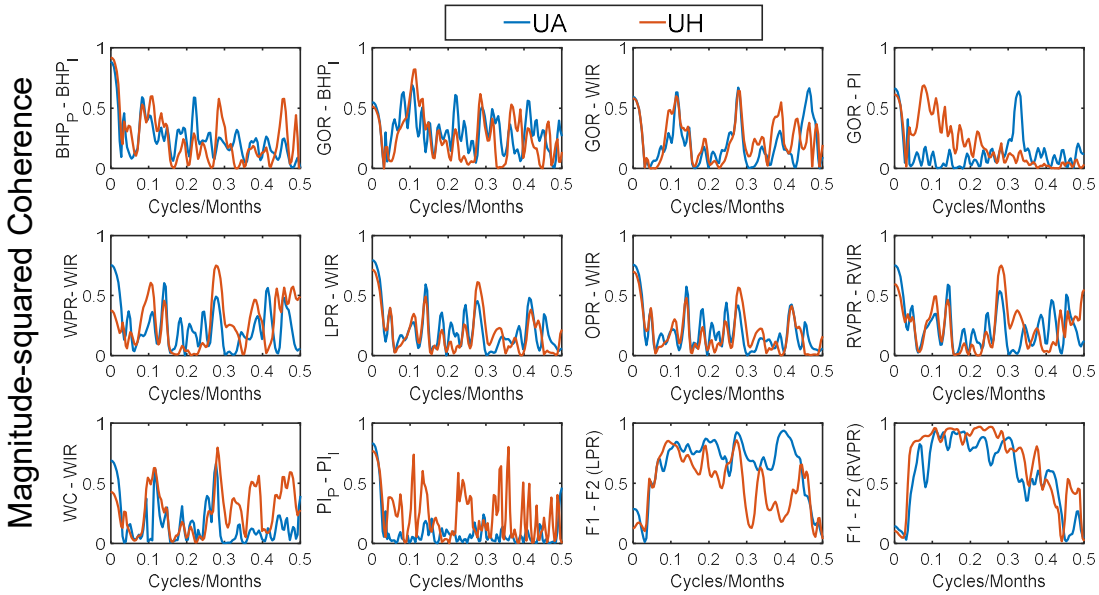

Figure 23. Magnitude-square coherence of various injector-producer well-variable pairs for the cases with heterogeneity effect.

4.6 Exploring the Informative Connectivity Indicators

The above examination of the cross-correlation coefficient, magnitude-squared coherence and periodogram profiles of these well-variable pairs reveals similar if not

superior information contents exist in the profiles based on $F1 - F2$ pair. Additionally, I observed indicators based on cross-correlation coefficients of the $F1 - F2$ pair consistently provided meaningful information on connectivity. One of the criteria used to decide on this is the extent to which the indicators can capture the change in reservoir conditions and well locations. Another factor was the ease of interpretation. Thus, I will illustrate the indicators based on cross-correlation coefficients of the $F1 - F2$ pair in greater detail. However, I have not determined the best indicator or the well-variable pair in this exploratory work. Technically, any of the well variable-pairs and indicators could be pursed further. And there are not yet solid criteria in choosing one over another.

Now, we can determine $F1 - F2$ functions several ways based on different production and injection rates. It will be difficult to examine all possible ways to infer connectivity indicators. Additionally, as discussed previously in the methodology section, there can be at least eight different connectivity indicators based on the cross-correlation coefficient profiles of well-variable pairs. Figure 24 displays cross-correlation coefficient profiles of $F1 - F2$ pair for the homogeneous cases with well-distance effect. Figure 24a displays $F1 - F2$ profiles based on water production and water injection rates; Figure 24b shows the profiles based on liquid production and water injection rates; Figure 24c those based on oil production and water injection rates; while Figure 24d based on reservoir-volume production and reservoir-volume injection rates. Blue line is the base case (UA), red line is the case with closer well distance (UA-CP1), and yellow line is the case with distant well distance (UA-DP1). Cross-correlation coefficients based on both negative and positive time-shifts are shown in these figures. Figure 24 suggests that cross-correlation coefficients based on negative time-shifts have a more pronounced effect of the subsurface

conditions. Moreover, because production rate in waterflood reservoir is controlled either by the total reservoir volume expansion due to reservoir depletion, or by the injection rate. Variables at reservoir conditions are believed to better reflect the true nature of reservoir properties. Thus, to keep the number of indicators to a manageable number, I decided to explore in greater detail the indicators based on cross-correlation coefficients only with negative time-shifts of the $F1 - F2$ pair using reservoir-volume production and injection rates.

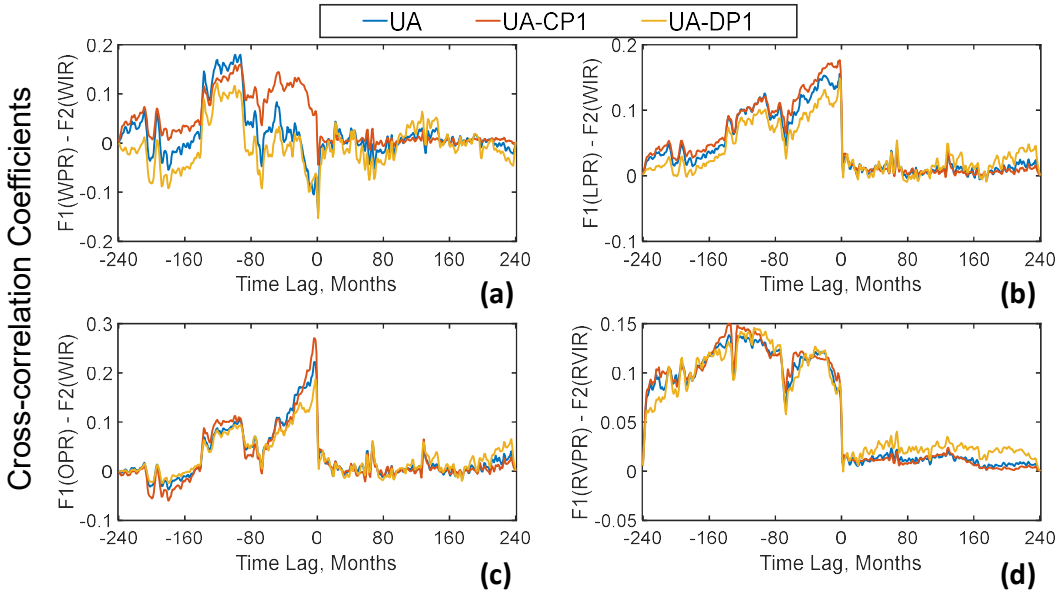

Figure 24. Cross-correlation coefficient profiles of $F1 - F2$ pair for the homogenous cases with well distance effect.

The reservoir-volume production rates and the cross-correlation coefficients profile using negative time shifts for the case with well distance effect is shown in Figure 25a and Figure 25b. UA is the base case (blue), UA-CP1 is the case with closer well distance (red), and UA-DP1 is the case with distant well distance (yellow). The reservoir rates maintained similar performance with the distance effect, only the close well distance case shows a higher production during the period when the injector is shut in. However, from Figure

25c, the streamline fraction of the injector in the three cases showed that the distant producer actually connects better with the injector, whereas the closer producer is the least connected one. I observed this information from the cross-correlation profile that obtained by smoothing the signals, as shown in Figure 25d. While the amplitudes of first peak (XC1A) and maximum peak (XC2A) is similar through the comparison cases, the lag of the first peak (XC1L) and maximum peak (XC2L) seems to give clues about the connectivity information that matches with streamline results.

The smoothing methods I attempted includes:

1. Savitzky-Golay finite impulse response smoothing filter, with the polynomial order ranging from 1 to 9, and frame length 3, 5, 7, 9 accordingly as it has to be odd and greater than polynomial order.
2. Moving average. It is a lowpass filter with filter coefficient equal to the reciprocal of the span. I tested the span ranging from 1 to 15.
3. Local regression. It uses the weighted linear least squares and a first degree of polynomial model. The weighted linear squares ranged from 0.01 to 0.1.

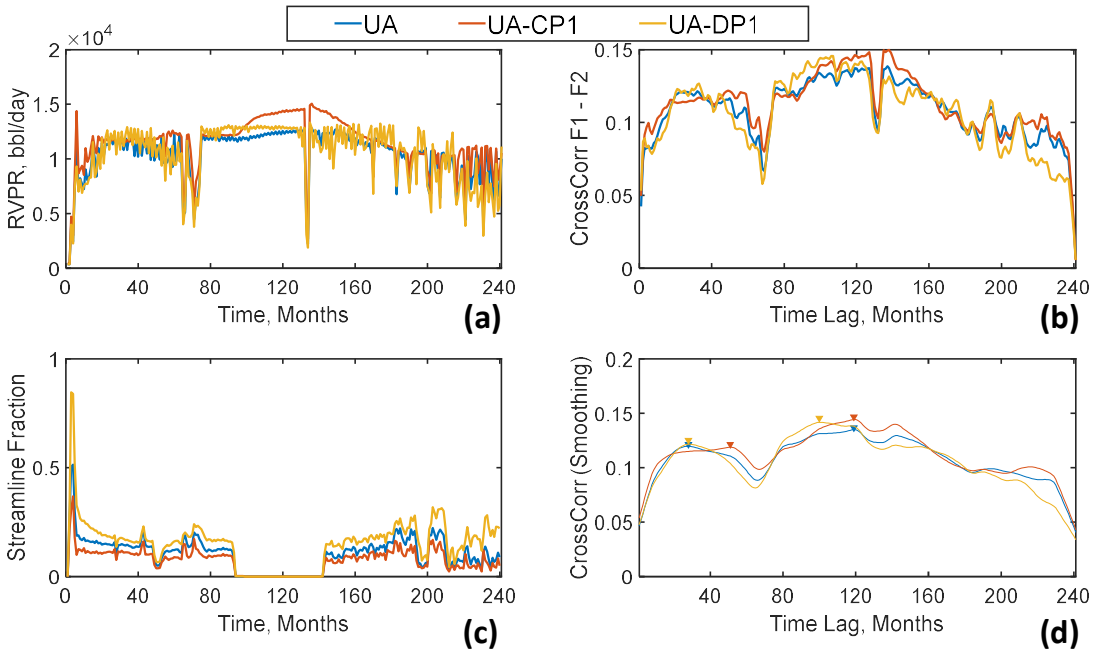

Figure 25. Effect of well distance variation on connectivity indicators. (a) reservoir volume production rate; (b) cross-correlation coefficient profiles; (c) streamline fraction of the injector; and (d) cross-correlation profiles after smoothing.

The reservoir-volume production rates for the homogeneous case (UA) and the layer-wise variation case (UL) is shown in Figure 26a. Figure 26b shows the corresponding cross-correlation coefficients using negative time-shifts. The blue line represents the base case, whereas the red line is the case with layer-wise variation. As evident in Figure 26d, cross-correlation coefficient profiles capture the effect of the layer-wise variation. There is a definite increase in the reservoir volume production rate of the layered case, but the streamline fraction in Figure 26c shows that the connectivity is lower in the beginning, and get higher after the shut-in period (in UL). The lag of the first peak (XC1L) and maximum peak (XC2L) seems to give clues about the connectivity information that matches with streamline results. It indicates that the response of the producer is delayed in the beginning (in UL) as compared to the base case, but the response with later time lag shows more connectivity in the later stage of production. However, the amplitudes of first peak (XC1A)

and maximum peak (XC2A) is significantly higher (in UL), which is suspected to be the influence of primary production, as the reservoir volume production is significantly higher. Thus the indicators of the amplitudes remain clouds, and need further investigation.

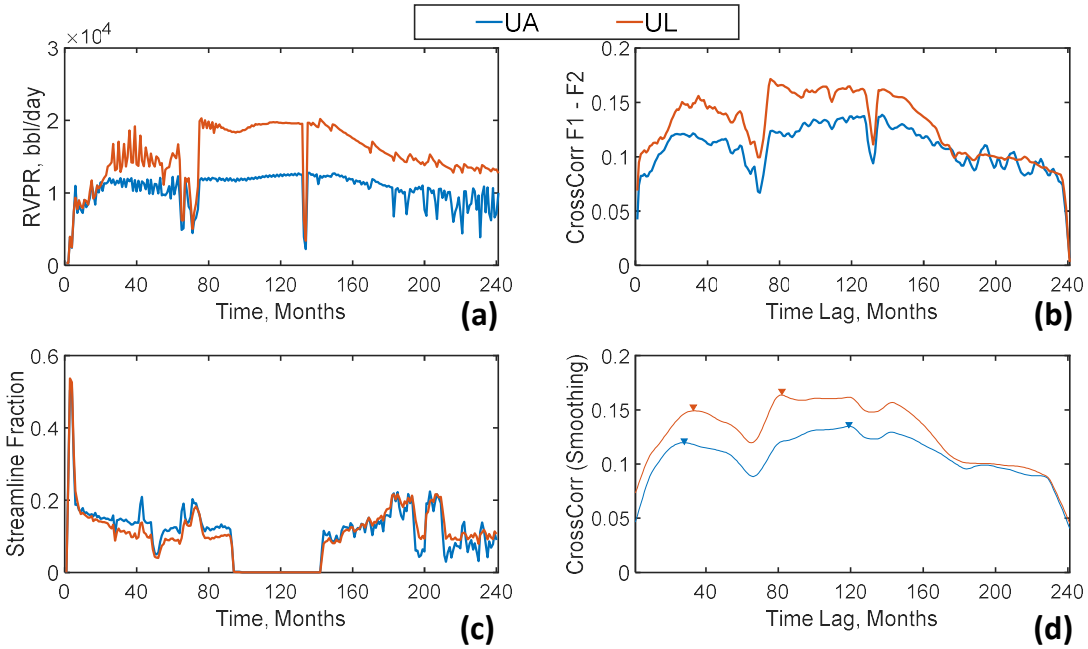

Figure 26. Effect of layer-wise property variation on connectivity indicators. (a) reservoir volume production rate; (b) cross-correlation coefficient profiles; (c) streamline fraction of the injector; and (d) cross-correlation profiles after smoothing.

Figure 27a shows the reservoir-volume production rates for the two-well homogenous case (UA) and the three-well case (UA-3W). Figure 27b shows the corresponding cross-correlation coefficient profiles using negative time-shifts. Figure 27c once again indicates a reverse result of the connectivity comparison from streamline fraction. The lag of the first peak (XC1L) again captures the faster response in the connectivity between injector-producer, indicating better connectivity. Notice here is that the maximum peak and the first peak (in UA-3W) is overlapped.

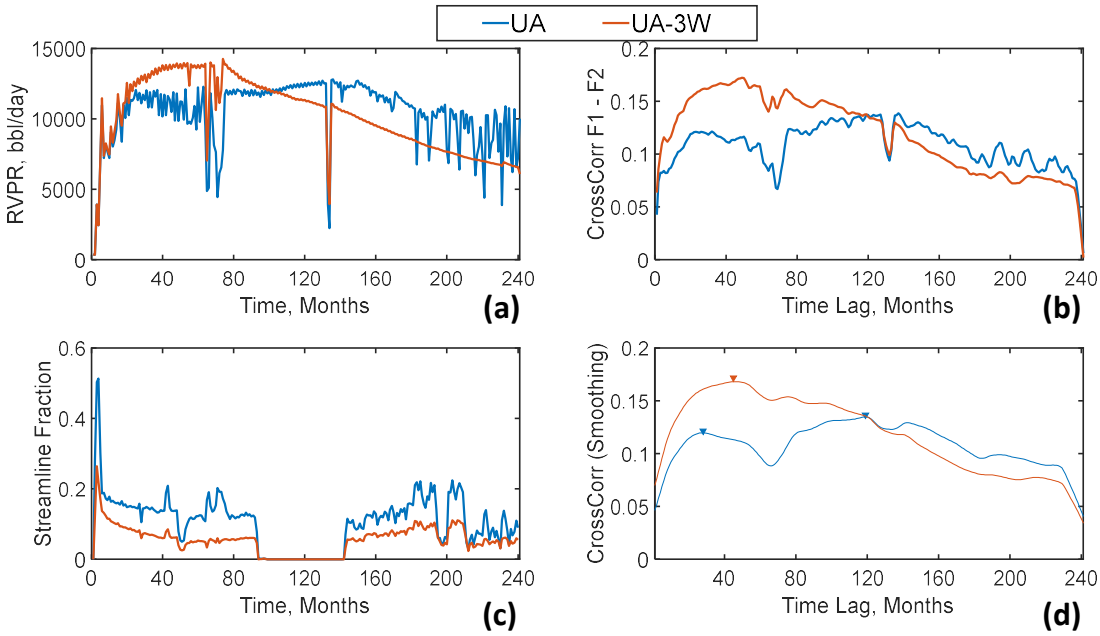

Figure 27. Effect of well interference on connectivity indicators. (a) reservoir volume production rate; (b) cross-correlation coefficient profiles; (c) streamline fraction of the injector; and (d) cross-correlation profiles after smoothing.

Figure 28a shows only the reservoir-volume production rates for the two-well case homogenous case (UA) and the heterogeneous case (UH). Figure 28b shows the corresponding cross-correlation coefficients using negative time-shifts. As shown in Figure 28d, the time lag of first peak (XC1L) again shows a shorter delay, indicating a faster response due to more connected with the producer (in UH). The maximum amplitude (XC2A) also shows a higher response, indicating a higher energy in production. The two indicators matches the result showed in streamline fraction (Figure 28c). I will examine heterogeneity effect in detail in a subsequent investigation.

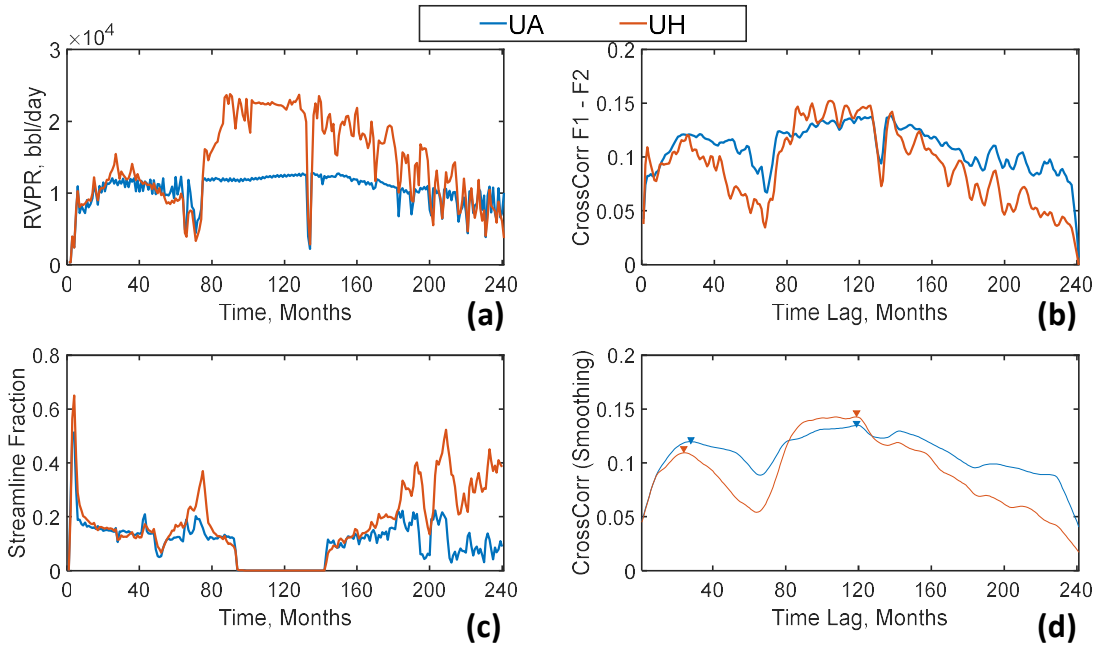

Figure 28. Effect of heterogeneous porosity and permeability on connectivity indicators. (a) reservoir volume production rate; (b) cross-correlation coefficient profiles; (c) streamline fraction of the injector; and (d) cross-correlation profiles after smoothing.

So far based on the simple two-well cases, I examined the injector-producer distance effect, the effect of layer-wise variation, the well-interference effect and the effect of heterogeneity. I examined connectivity indicators based on the three signal-processing methods, and further explored in details about cross-correlation coefficients using negative time-shifts with $F1$ and $F2$. In the following chapter, I discuss more complex multi-well realistic reservoir scenarios undergoing waterflood.

Chapter 5: Realistic Multi-well Scenarios

In this chapter, I used realistic reservoir scenarios with multiple wells undergoing waterflood to demonstrate the application of the connectivity indicators described previously. I will introduce the construction of the reservoir model first, and then I will show the cross-correlation coefficients and magnitude-squared coherence profiles for the multi-well scenarios.

5.1 Reservoir Model Construction for Multi-well Scenarios

Reservoir rock and fluid parameters and operational practices modeled here are characteristic of Permian-basin. Statistics and the data ranges utilized in this study came from a previous compilation presented in Ordonez et al. (2018). The geological base case uses median value of the rock and fluid properties, as shown previously in Table 2. The top of the structure is at a depth of 5,100 ft and the bottom of the structure at 5,300 ft. The model included 114,800 cells (144×150×53) in a 7,200 ft × 7,500 ft grid.

The reservoir consists of four zones with different formation properties. The upper interval constitutes the high-quality zone with high porosity and high permeability; the middle zone consists of a shale barrier zone with low porosity and very low permeability; lower and bottom zone has intermediate porosity and permeability. The petrophysical models are constructed by Sequential Gaussian simulation for all zones. The distribution methods and data range for porosity and permeability models in base case are the same with the previous heterogeneous case for simple two well scenario, as shown in Table 5. The permeability model further uses co-kriging method, from the heterogeneous porosity model. The estimated collocated co-kriging coefficient is kept constant as 0.8.

Figure 29 presents the model schematic. I considered nine producers and six injectors in the waterflood. The relative locations of these wells are shown in Figure 30.

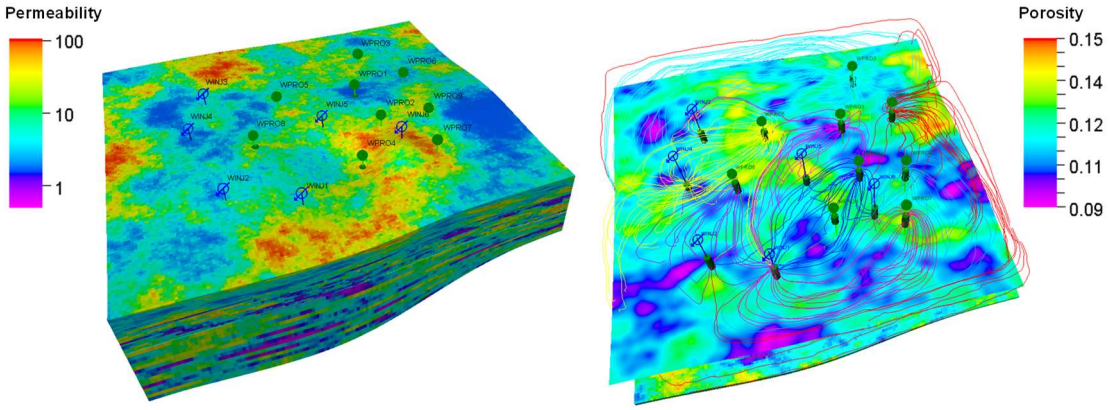

Figure 29. Schematic of the realistic multi-well reservoir cases characteristic of Permian-specific reservoir and fluid properties and operational practices. (a) 3D model displaying the 4 zones (upper, middle, lower and the bottom), (b) streamlines with water saturation over a draped map of average porosity. Nine producers and six injectors are active in the field.

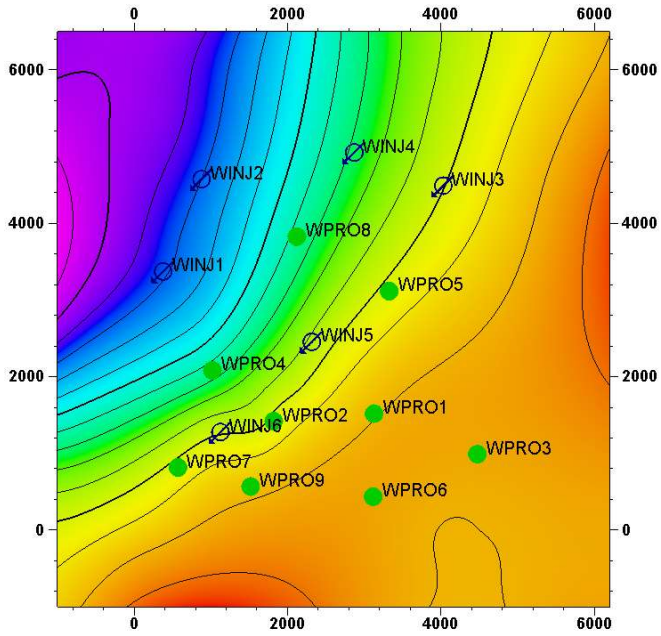

Figure 30. Schematic of relative well locations. The contours in the background are based on the elevation of the bottom surface.

I performed streamline simulations using a commercial simulator (Schlumberger 2016) for 20 years using historical rate controls (injectors using water injection rate and producers using oil production rate) and bottom-hole pressure limits, same as the simple two-well scenarios. The rates come from a realistic water-injection field from Permian basin. Therefore, all the data from the simulation contains a lot of fluctuations. These kind of fluctuations are necessary for performing signal-processing methods. The operating conditions like shut-in the injection or production are not excluded from the data. For example, Injector 5 contains about 10 months of shut-in period in the middle of simulation time-frame. The goal is to observe how the signal-processing methods respond to these operating changes.

To capture the uncertainty in heterogeneous and complex reservoir conditions, I explored Design of Experiments using over 40 static and dynamic parameters. Working with large number (40) of uncertain variables is a daunting undertaking. In order to manage the size of sampling, I used the most compact sampling design known as Plackett-Burman (PB) (Plackett and Burman, 1946) and as well as a space-filling Monte-Carlo method or Latin-hypercube (LHS) (Iman et al., 1980). For multi-variate uncertain inputs, different methods of DoE can help sample results across all possible values within the range. Monte-Carlo method generates good degree of randomness but may result in non-uniform or clustered sampling. LHS overcomes this shortcoming by spreading the sample points more evenly. PB sampling utilizes the extreme values of all uncertain variables (either the minimum or the maximum), which helps to identify the most significant parameters and deepen their impacts on the model. Table 6 itemizes the range of the uncertain parameters used in the study. The uncertainty cases examined cover a good variety of realistic

production-injection scenarios. Figure 31 shows the cumulative water injection and liquid production rate profiles for all the uncertainty cases.

Uncertain Parameters	Range	
	Minimum	Maximum
Transmissibility multiplier (middle zone)	0.01	10
Porosity permeability coefficient	0.6	0.8
Minimum porosity (upper zone)	0.025	0.06
Minimum porosity (middle zone)	0.015	0.05
Minimum porosity (lower zone)	0.02	0.055
Maximum porosity (upper zone)	0.2	0.25
Maximum porosity (middle zone)	0.085	0.14
Maximum porosity (lower zone)	0.18	0.23
Minimum permeability (upper zone)	0.5	2.5
Minimum permeability (middle zone)	0.1	1
Minimum permeability (lower zone)	0.25	2
Maximum permeability (upper zone)	100	120
Maximum permeability (middle zone)	5	10
Maximum permeability (lower zone)	60	80
Oil-water contact depth (ft)	-5,350	-5,265
Capillary pressure at WOC depth (psi)	0	6
Oil density (°API)	25	40
Solution GOR (Mscf/STB)	0.05	1.5
k_v/k_h ratio (lower zone)	0.01	0.5
k_v/k_h ratio (upper zone)	0.01	0.5
Water saturation at P_c = 0 psi	0.55	0.64
Critical water saturation	0.15	0.4
Residual oil saturation	0.15	0.35
Gas specific gravity	0.6	0.7
Rock compressibility (psi^{-1})	2.00E-06	5.00E-05
Critical gas saturation	0	0.1
Water salinity (ppm)	50,000	120,000
Major direction of Anisotropy (upper zone)	550	2150
Vertical direction of Anisotropy (upper zone)	6	40
Vertical direction of Anisotropy (lower zone)	7	20
Nugget of variogram	0.0001	0.01
Azimuth of major direction (°) (upper zone)	-30	60
Azimuth of major direction (°) (lower zone)	-75	15

Table 6. Some uncertainty parameters used in the multi-well reservoir scenarios.

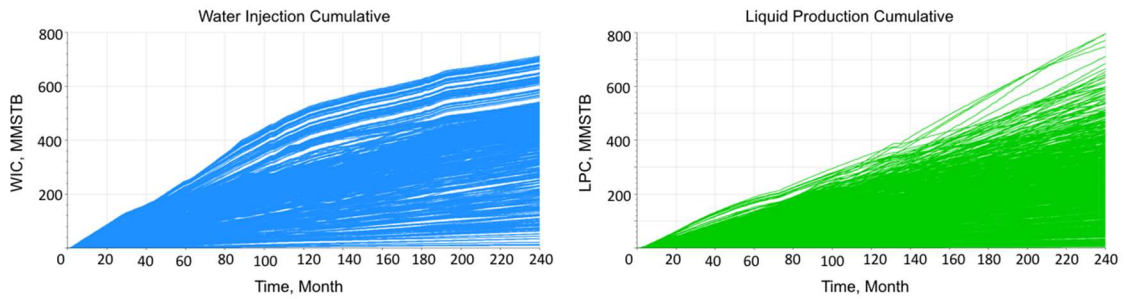

Figure 31. Uncertainty in production scenarios examined in the multi-well study: (a) water injection cumulative with time, (b) liquid production cumulative with time.

5.2 Application of Digital Signal-processing Methods to Multi-well Scenarios

The multi-well cases contained six injectors and nine producers. Through more than one hundred uncertainty DoE cases, I could examine a large range of pair-wise connectivity scenarios affected by different geological conditions and reservoir properties. As an illustration, Figure 32 displays cross-correlation coefficient profiles with negative time-shifts of the $F1 - F2$ pair based on reservoir-volume injection and production rates from one of the multi-well simulation cases. The nine plots are for the nine producers active in the waterflood. For each subplot, y-axis is the cross-correlation coefficients, and x-axis is time lag in months. Each plot contains six curves corresponding to six injectors, wherein peaks appeared. Peaks are indicated through all curves. As suggested previously, I examined the connectivity indicators based on the first peak and the maximum peak.

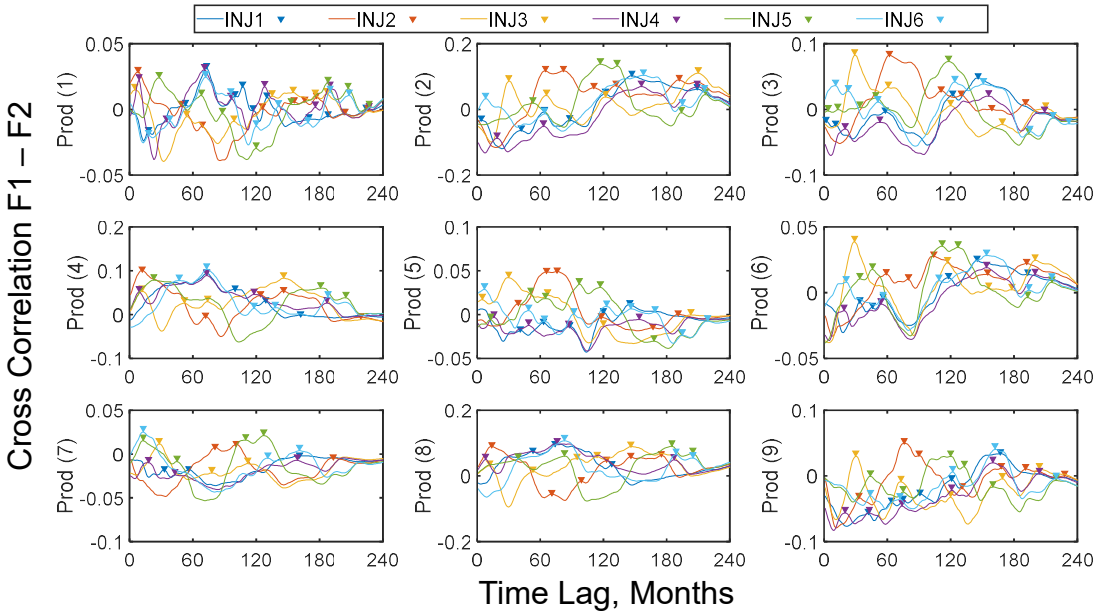

Figure 32. Cross-correlation coefficient profiles with negative shifts of $F1 - F2$ pair based on reservoir-volume injection and production rates from one of the multi-well simulation cases.

It is worth noticing that there are periods of negative cross-correlation coefficients of $F1$ and $F2$ for all the injector and producer pairs. How to interpret these negative correlation coefficients? Let me revisit the connotations of $F1$ and $F2$. $F1$ identifies the decline in production rates with time for a particular producer in an injector-producer couplet system, while $F2$ is the net withdrawal from that couplet system. In a realistic multi-well system for many reasons (changes in operational and reservoir dynamical conditions), the net withdrawal from an injector-producer couplet can vary. It can decrease or increase over time. Although the injector-producer is communicating, there may not be corresponding changes in the producer rate or pressure decline that directly affects $F1$. Under these conditions, other contributing and communicating injectors dominate the performance of the producer in focus. Additionally, abrupt operational change causes extreme spikes in the data, resulting in its derivative to waver from the positive side to the negative and vice versa. Thus, these negative coefficients with large values could indicate two time-series are out of phase (peaks aligned with troughs).

Similar to the above cross-correlation profiles, Figure 33 displays magnitude-squared coherence profiles based on reservoir-volume injection and production rates from one of the multi-well simulation cases. For each subplot, y-axis is the squared-magnitude at each frequency, and x-axis is frequency in cycles/months. For multi-input and multi-output systems (multiple injector and multiple producers), the multiple-coherence function becomes:

$$C_{Ij_n}(f) = \frac{P\dagger_{Ij_n}(f) P_{II}^{-1}(f) P_{Ij_n}(f)}{P_{j_n j_n}(f)}$$

$$= \left[P^*_{i_1 j_n}(f) \dots P^*_{i_m j_n}(f)\right] \begin{bmatrix} P_{i_1 i_1}(f) & P_{i_1 i_2}(f) & \cdots & P_{i_1 i_m}(f) \\ P_{i_2 i_1}(f) & P_{i_2 i_2}(f) & \cdots & P_{i_2 i_m}(f) \\ \vdots & \vdots & \ddots & \vdots \\ P_{i_m i_1}(f) & P_{i_m i_2}(f) & \cdots & P_{i_m i_m}(f) \end{bmatrix}^{-1} \begin{bmatrix} P_{i_1 j_n}(f) \\ \vdots \\ P_{i_m j_n}(f) \end{bmatrix} \frac{1}{P_{j_n j_n}(f)}$$

(7)

For the nth producer, I corresponds to m producers. P_{Ij_n} is the vector of cross-power spectral densities between the injectors and producer j_n; P_{II} is a matrix of the power-spectral densities and cross-power spectral densities of the injectors. $P_{j_n j_n}$ is the power-spectral density of the producer j_n. The dagger † stands for the complex conjugate transpose. I examined the connectivity indicators based on the eigen-frequency (MSC1) and the maximum magnitude (MSC2). The reason I am pursuing the similarity measurements in frequency domain here, is to provide a thorough exploratory work, with the purpose of capturing potential information hidden in the signals. Analyses in frequency domain for reservoir characterization is standard in geophysical and seismic processing (Marfurt, 1984).

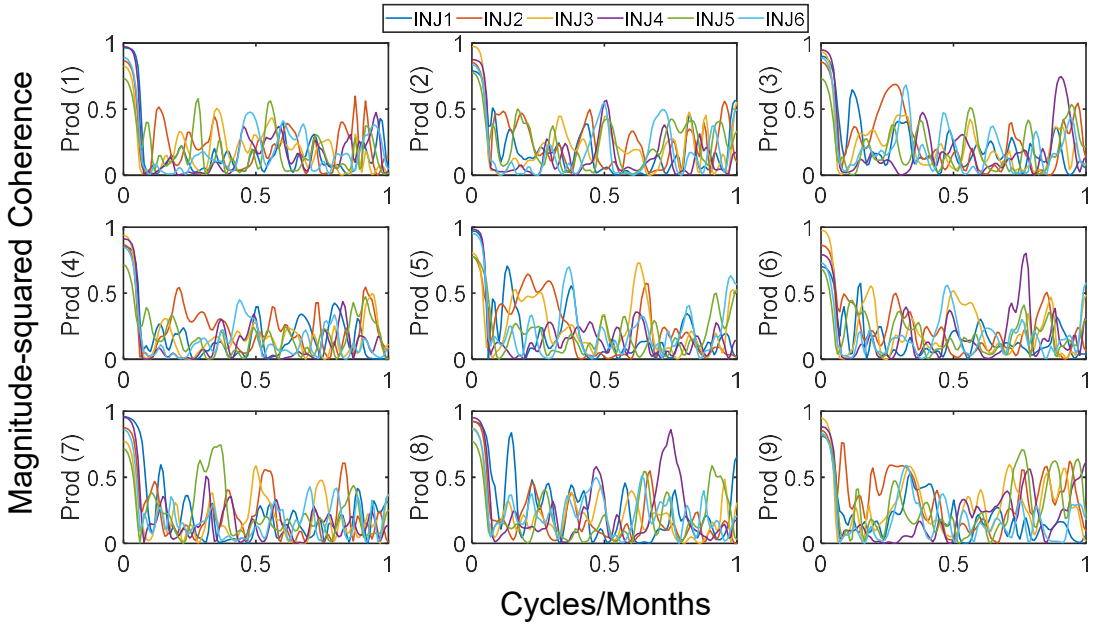

Figure 33. Magnitude-squared coherence profiles with negative shifts of $F1 - F2$ pair based on reservoir-volume injection and production rates from one of the multi-well simulation cases.

I also studied the injector-to-producer streamline-based allocation fractions, as shown in Figure 34. The streamline-based allocation fractions are extracted from the simulation cases, and plotted based on the fractions connected to the producers. For each subplot, y-axis is the streamline fractions, and x-axis is production time in months.

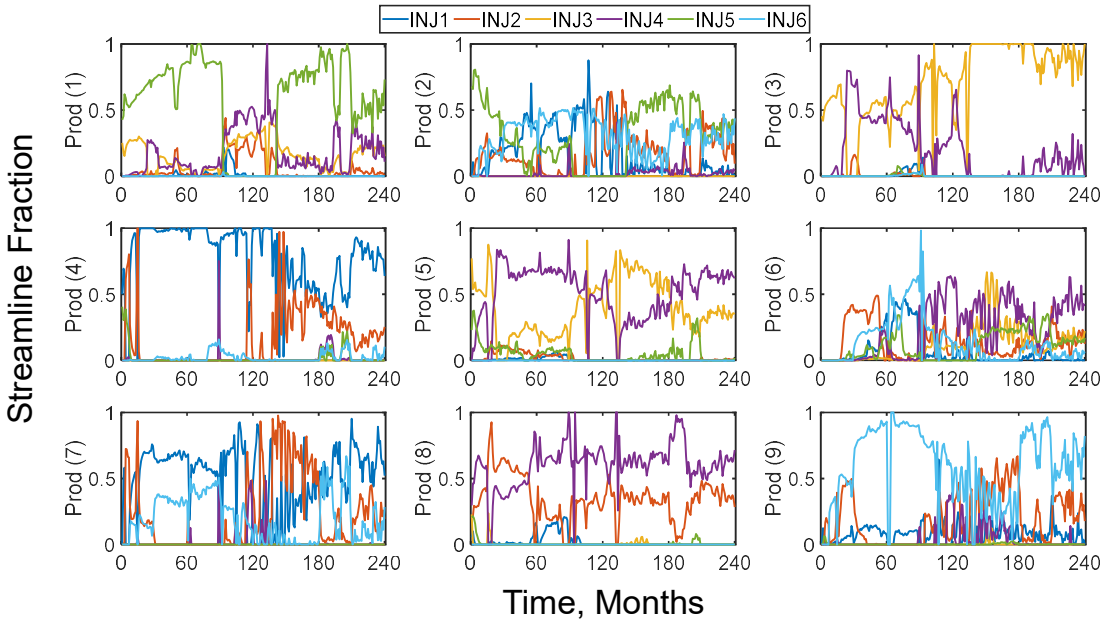

Figure 34. Injector-to-producer streamline allocation fractions for the same simulation case corresponding to the above figure.

The cross-correlation coefficients, MSC and streamline fractions profiles are from same case, among all the uncertainty cases. In order to visualize how the methods are comparing with the streamline simulation results, Figure 35 shows the three profiles for Producer 2. From Figure 35a, the lag of first peak (XCL1) shows Injector 1 connects the best with this producer, and Injector 6 is the next. The amplitude of maximum peak (XCA2) indicates Injector 5 connects well with Producer 2. Injector 2 also have relatively high amplitude at the maximum peak, and smaller lag at the maximum peak. It is suspected to reveal a temporal evolution of the connectivity through time (Injector 2 connects better with Producer 2 at an earlier time, and then Injector 5 connects better with Producer 2). From Figure 35b, the Magnitude-squared coherence profile failed to show a standout eigen frequency (MSC1) and associated amplitude (MSC2). But if we take the well that has the highest MSC1 and MSC2 value, it would be Injector 2. If we treat the streamline as the

fact, Figure 35c shows that through time, Injector 1, 2, 5 and 6 indeed are connected well with Producer 2 throughout production.

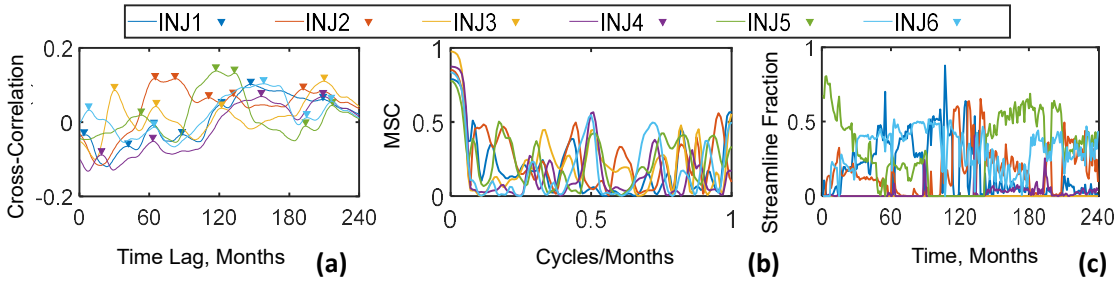

Figure 35. Comparison of (a) cross-correlation coefficient, (b) Magnitude-squared coherence and (c) streamline allocation fractions profiles for Producer 2.

To view another example for the case, Figure 36 displays the three profiles for Producer 6. From Figure 36a, the lag of first peak (XCL1) shows Injector 4 connects the best with this producer, and Injector 6 is the next. The amplitude of maximum peak (XCA2) indicates Injector 5 connects well with Producer 6. Injector 2 and Injector 6 have similar high amplitude at the maximum peak, which might be the evidence of they are both connected with Producer 6, and they are competing with each other. If we take a look of Figure 36b, the Magnitude-squared coherence profile shows a high standout eigen frequency (MSC1) and associated amplitude (MSC2) of Injector 4. Injector 6 ranks the next. This matches with what we observe from XCL1 in cross-correlation coefficients profile. Again, we treat the streamline as the fact to conduct comparison. Figure 36c shows that through time, Injector 4 and Injector 6 indeed are connected well with Producer 6 throughout production life. The results match with the observation from signal-processing method-based indicators.

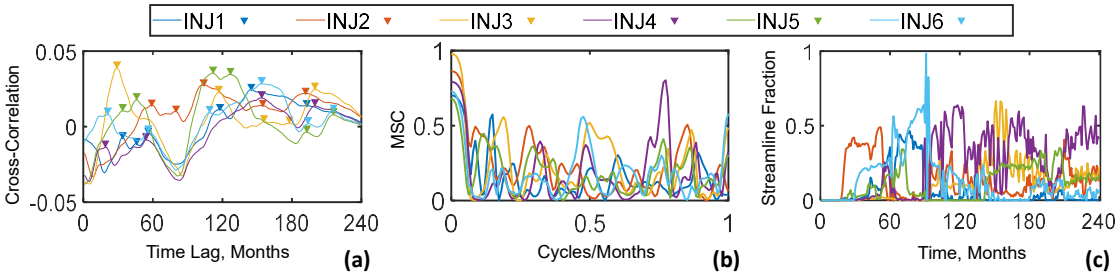

Figure 36. Comparison of (a) cross-correlation coefficient, (b) Magnitude-squared coherence and (c) streamline allocation fractions profiles for Producer 6.

The above examples prove connectivity indicators based on cross-correlation and MSC are able to give information about connectivity. However, it is true that not all the observation from the signal-processing profiles match with the streamline results. One inevitable reason would be the streamlines connected to the producers do not just emanate from the injectors alone. Figure 37 shows an example of the streamlines representing the driving energy. It is worth noticing that the primary recovery still exists as the streamline representing expansion energy contributes to the total streamlines. If we take a look at the streamline fraction at the last time step of the simulation, as shown in Figure 38, several producers have large portions of production coming from the support of natural energy. It would result in reservoir volume production rate of a particular producer to be significantly higher than the total streamline rates. And this is suspect to be a cause of our connectivity indicators, who utilized reservoir volume production rates, result in different interpretation of connectivity between wells. Additionally, we cannot ignore the influence of the complexity in the reservoir architecture and the flow dynamics. Correspondence of the streamline fractions and connectivity indicators is not always of high quality. However, as illustrated by Figure 35 and Figure 36, these indicators are able to provide thoughtful insights into the interwell connectivity.

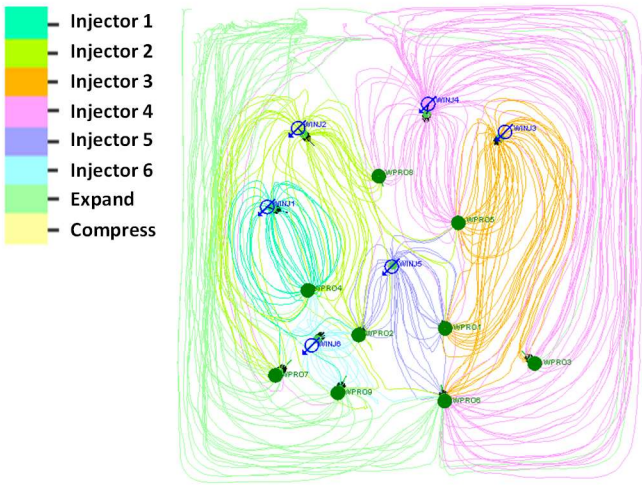

Figure 37. Schematic example of streamlines connected to injectors and reservoir.

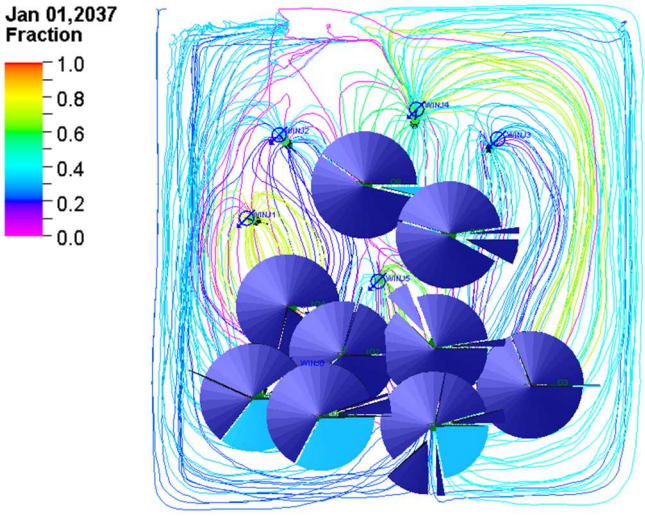

Figure 38. Example of streamline fraction at the end time step of simulation for multi-well scenarios.

In the following chapter, I will explore comparative analysis in the statistical sense of the proposed connectivity indicators against streamline-based injector-to-producer allocation fractions and the injector-producer weight coefficients from the capacitance-resistance model.

Chapter 6: Comparison Study: Streamline Simulation

In this thesis, I proposed several connectivity indicators based on digital signal-processing techniques. To examine the quality these indicators, I compare them with injector-to-producer streamline-based allocation fraction. This chapter presents a comparison study using statistical diagnostic tools applying to over a hundred cases. These allocation fractions are the truth case as they reflect the exact fluid flow communication between injector-producer in the simulated synthetic cases.

Connectivity between any producer-injector pair is not static over the entire life of the reservoir. Depending on the well-operating conditions and the reservoir architecture, streamlines evolve during the life of the field. I compared the proposed indicators based on cross-correlation coefficients against mean streamline-based allocation fractions for each injector-producer pair. Figure 39, Figure 40, Figure 41 and Figure 42 illustrate the comparison of connectivity indicator and the mean injector-to-producer streamline-based allocation fractions. The indicators are based on the amplitude (XC1A) and time lag (XC1L) of cross-correlation coefficients using negative time-shifts at the first peak; the amplitude (XC2A) and time lag (XC2L) cross-correlation coefficients using negative time-shifts at the maximum peak, respectively. There are 6×9 scatterplots for all the pairs from nine producers and six injectors based on all the DoE simulation cases examined. The text box on the upper right corner of each subplot shows the correlation coefficient of the scatterplot. A high value of the correlation coefficient indicates proper alignment between the proposed indicator and the streamline fractions. For instance, Injector 6 is well connected to Producer 6, and the proposed indicator corresponds well with streamline fraction.

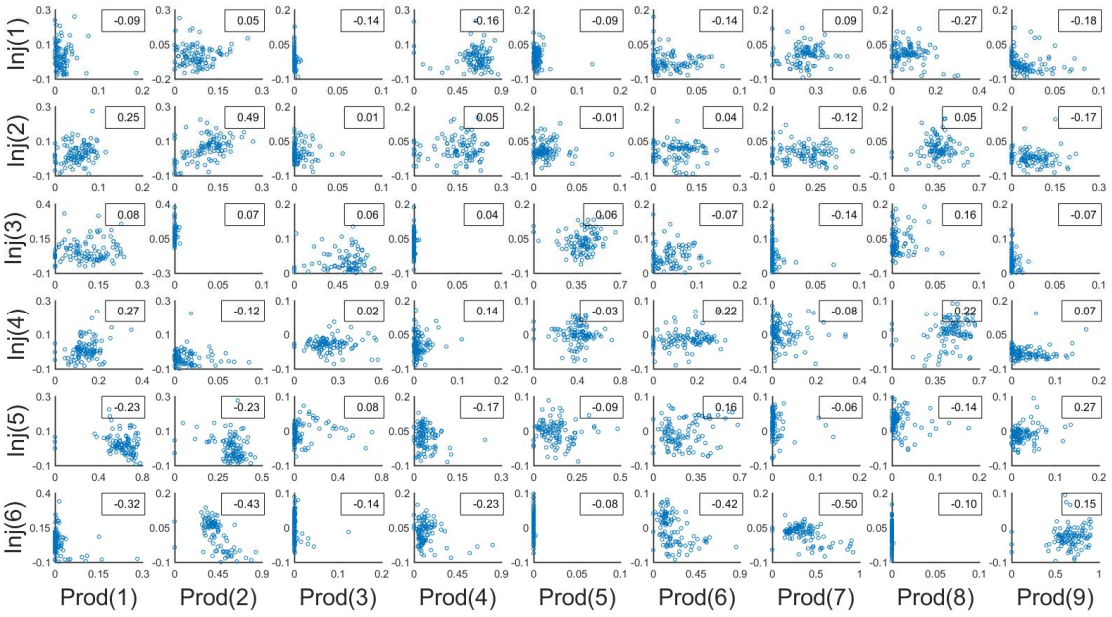

Figure 39. Comparison of connectivity indicator based on the cross-correlation coefficients using negative time-shifts at the first peak (XC1A) and the mean injector-to-producer streamline-based allocation fractions.

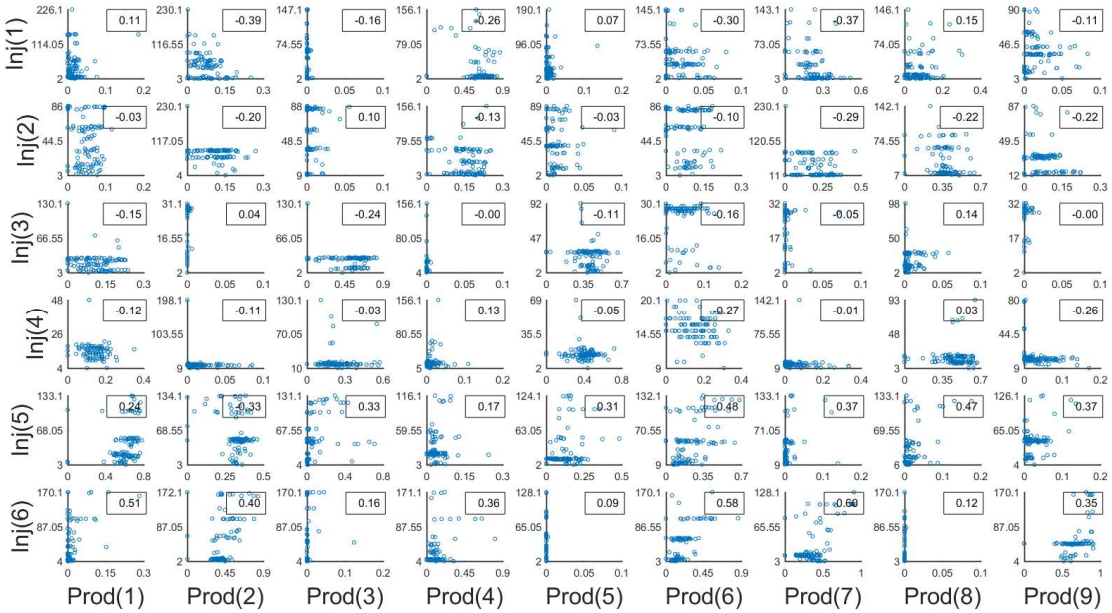

Figure 40. Comparison of connectivity indicator based on the time lag of cross-correlation coefficients using negative time-shifts at the first peak (XC1L) and the mean injector-to-producer streamline-based allocation fractions.

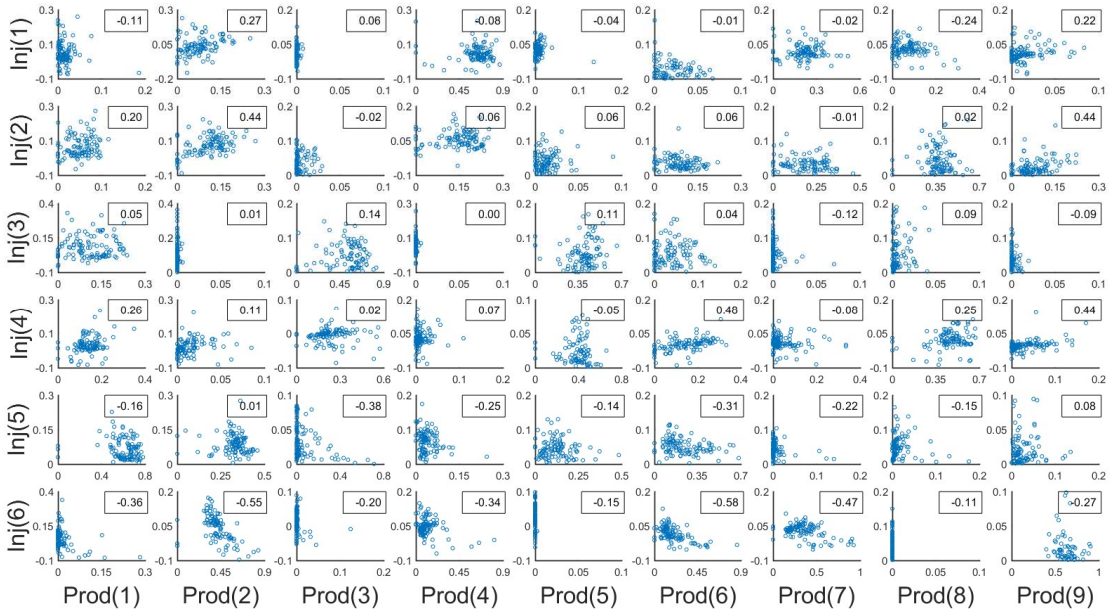

Figure 41. Comparison of connectivity indicator based on the cross-correlation coefficients using negative time-shifts at the maximum peak (XC2A) and the mean injector-to-producer streamline-based allocation fractions.

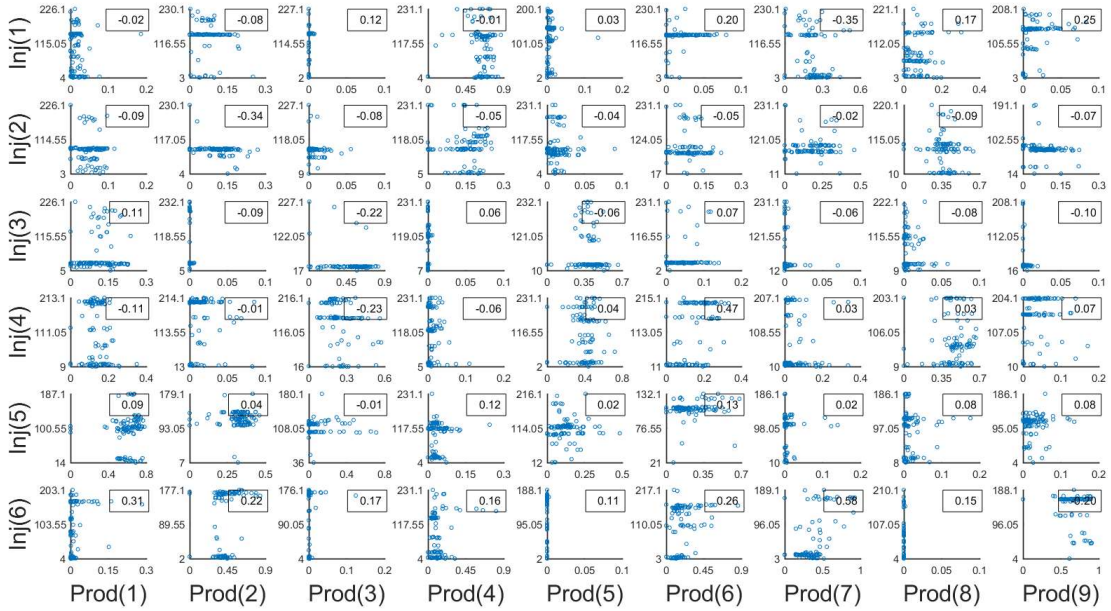

Figure 42. Comparison of connectivity indicator based on the time lag of the cross-correlation coefficients using negative time-shifts at the maximum peak (XC2L) and the mean injector-to-producer streamline-based allocation fractions.

I used heatmaps of the correlation coefficients between mean streamline fractions and all four indicators based on cross-correlation coefficients using negative time-shifts.

Figure 43 displays the heatmaps. The high value (in dark color) indicates a significant correlation between streamline fractions and the proposed indicators. The first peak can be considered as the first signal of communication between the producer and the injector, according to the cross-correlation for $F1 - F2$. The associated lag here is the time delay for the response signal. Because of the different fluid and rock properties of reservoir area between injector and producer, the response is not instantaneous. Thus, the time delay of the response can be a good indicator to evaluate the connectivity. The amplitude of the first peak can be interpreted as the energy response in the initial period of production. Based on the heatmaps shown in Figure 43, I can identify high-connectivity pairs like Injector 5 – Producer 1, Injector 6 – Producer 2, Injector 2 – Producer 4, Injector 6 – Producer 6, and Injector 6 – Producer 7.

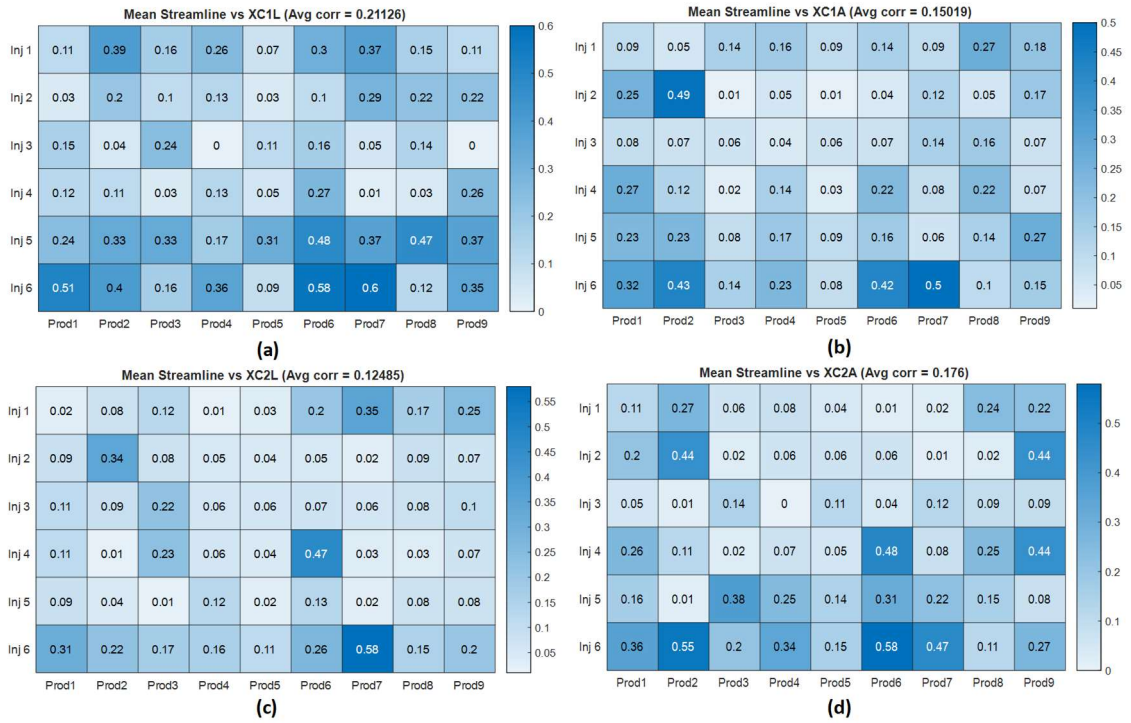

Figure 43. Heatmaps of the correlation coefficient of the scatter between mean streamline fractions and the proposed indicators based on cross-correlation coefficients using negative time-shifts. (a) Mean streamline fraction vs XC1L; (b) mean streamline fraction vs XC1A; (c) mean streamline fraction vs XC2L; (d) mean streamline fraction vs XC2A.

Chapter 7: Comparison Study: Capacitance-Resistive Model

This chapter presents a comparison study based on capacitance-resistive model. Capacitance-resistive model, as a popular mainstream tool for inferring interwell connectivity, also utilize well data that can be obtained from production. This study applied two solutions using two different control volumes. Figure 44a and Figure 44b show the schematic of drainage volume of a producer, and drainage volume between each producer and injector pairs, respectively. The results are given by connectivity fractions that represent the steady-state fractions of the rate of injector to producer. Compared to CRMP, which need to solve one time constant, one initial production, and one productivity index, CRMIP requires solving $N_{inj} \times N_{pro}$ of those unknowns.

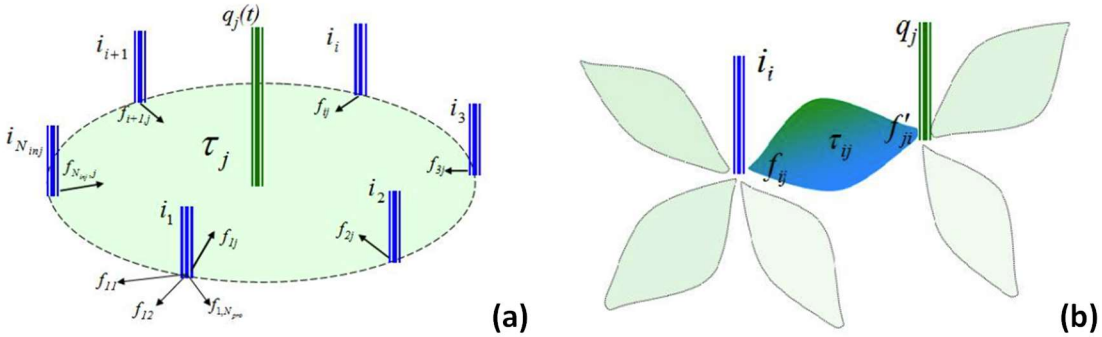

Figure 44. Schematic of control volume represented by (a) around producer, CRMP, and (b) between each producer/injector pair, CRMIP.

Because the definition for CRM connectivity fractions are conceptually align with the streamline allocation factors, I performed a similar comparison with the CRM-based connectivity measures. I explored how the CRM weight functions compare against the mean streamline fractions to begin with. Figure 45a shows one of the matches of reservoir-volume production rate from one of the simulation cases. Figure 45b displays the heatmap of the correlation coefficient between CRM-based weight-function with mean streamline

fractions. Interesting to note that overall correspondence of the CRM-based weight functions and the streamline fractions is poor.

Despite this, I compared the CRM-based weight functions against the proposed connectivity indicators based on cross-correlation coefficients using negative time-shifts. As shown in Figure 46, Figure 47, Figure 48 and Figure 49, these indicators are based on the amplitude (XC1A) and time lag (XC1L) of cross-correlation coefficients using negative time-shifts at the first peak; the amplitude (XC2A) and time lag (XC2L) cross-correlation coefficients using negative time-shifts at the maximum peak, respectively. Figure 50 illustrates the comparison of the capacitance-resistance model (CRM)-based weight coefficients and the mean injector-to-producer streamline-based allocation fractions. There are 6×9 scatterplots for all the pairs from nine producers and six injectors based on all the DoE simulation cases. The text box on the upper right corner of each subplot shows the correlation coefficient of the scatterplot. Figure 51 displays the heatmaps of the correlation coefficients between CRM-based weight coefficients and all four indicators based on cross-correlation coefficients using negative time-shifts.

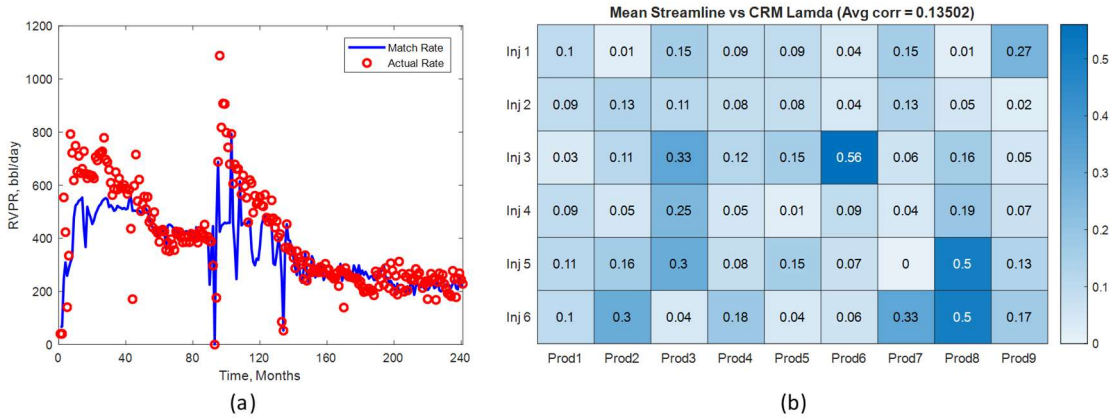

Figure 45. Comparison of capacitance-resistance model (CRM)-based connectivity with mean streamline fractions. (a) As an illustration, the match of reservoir-volume production rate for one producer, (b) heatmap of the correlation coefficient between capacitance-resistance model (CRM)-based weight-function with mean streamline fractions.

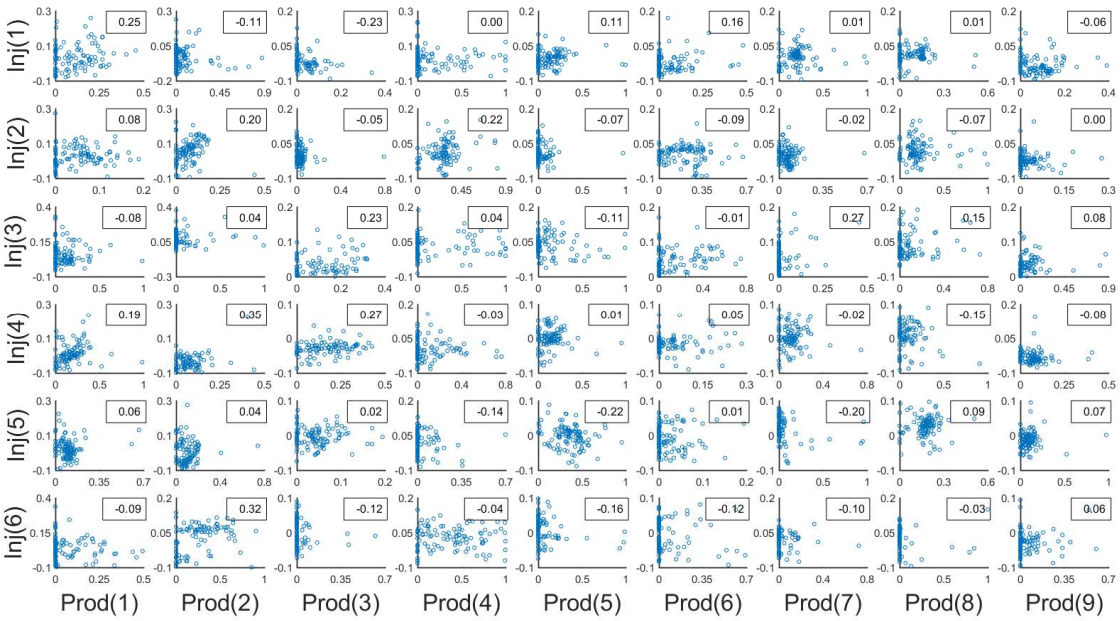

Figure 46. Comparison of the capacitance-resistance model (CRM)-based weight functions and the amplitude (XC1A) of cross-correlation coefficients using negative time-shifts at the first peak.

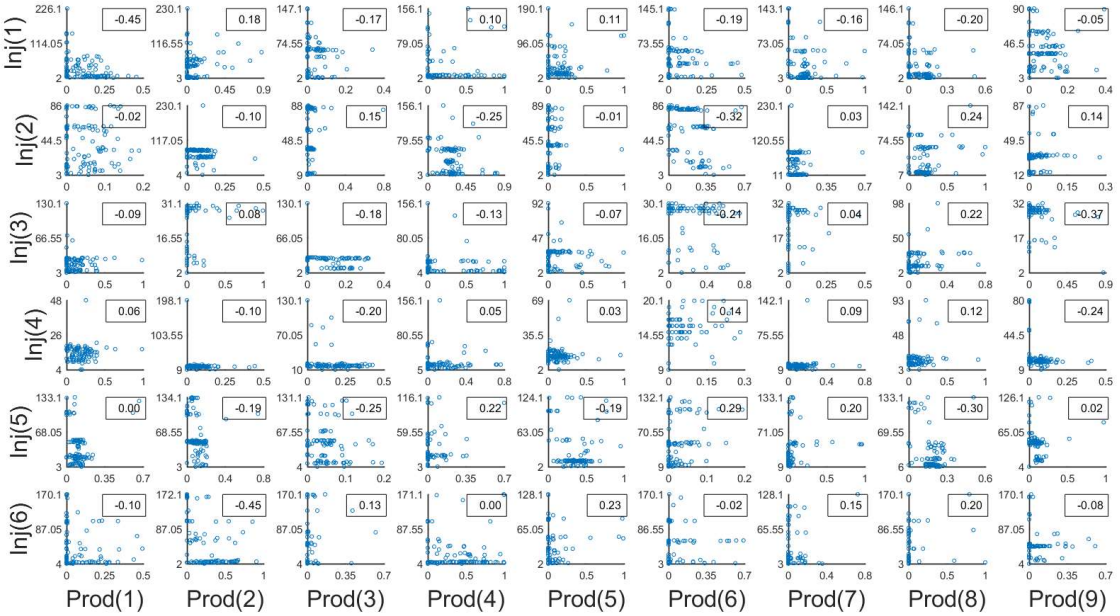

Figure 47. Comparison of the capacitance-resistance model (CRM)-based weight functions and the time lag (XC1L) of cross-correlation coefficients using negative time-shifts at the first peak.

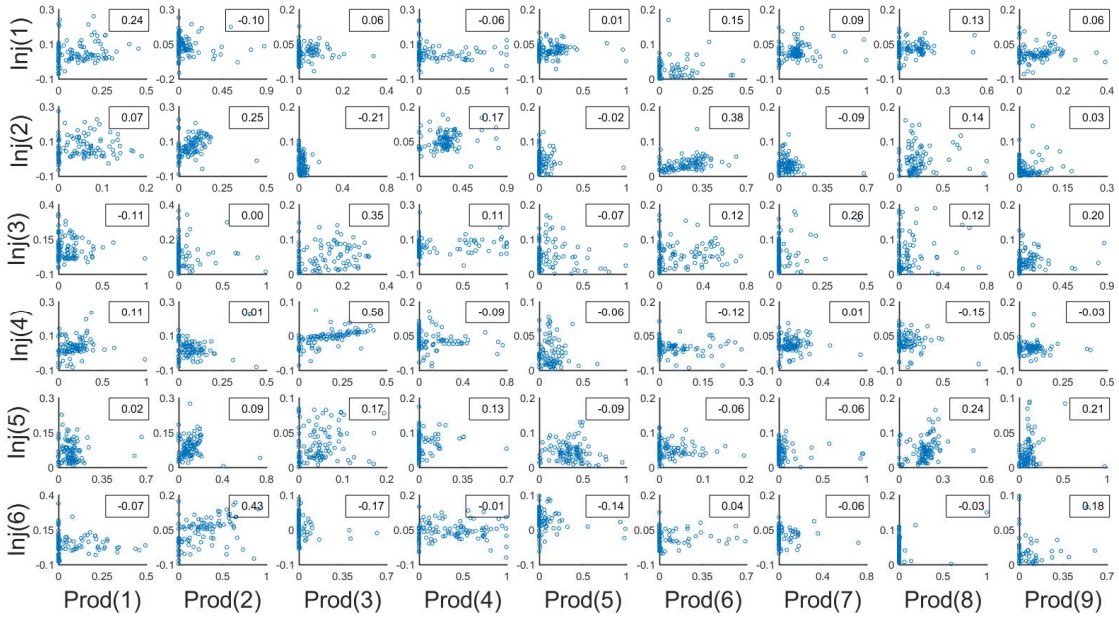

Figure 48. Comparison of the capacitance-resistance model (CRM)-based weight functions and the amplitude (XC2A) of cross-correlation coefficients using negative time-shifts at the maximum peak.

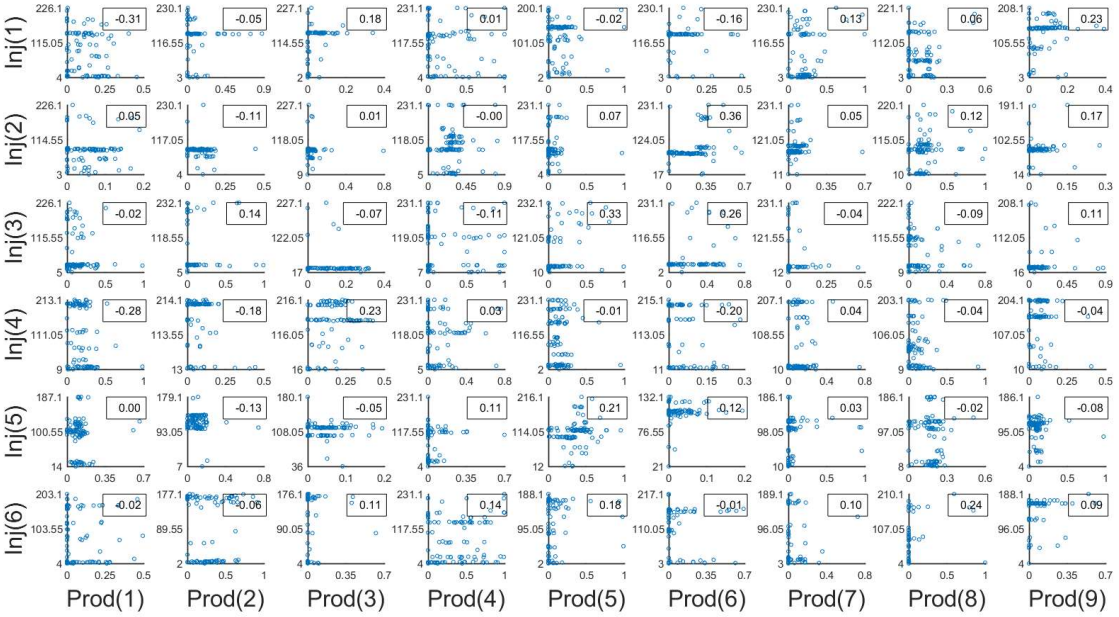

Figure 49. Comparison of the capacitance-resistance model (CRM)-based weight functions and the time lag (XC2L) of cross-correlation coefficients using negative time-shifts at the maximum peak.

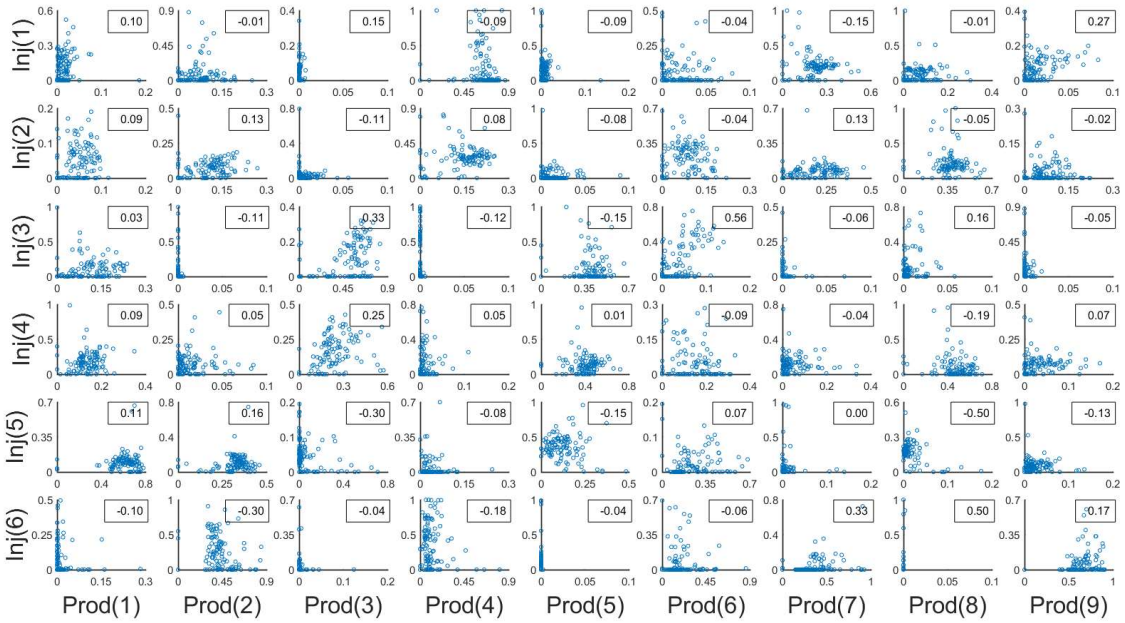

Figure 50. Comparison of the capacitance-resistance model (CRM)-based weight functions and the mean injector-to-producer streamline-based allocation fractions.

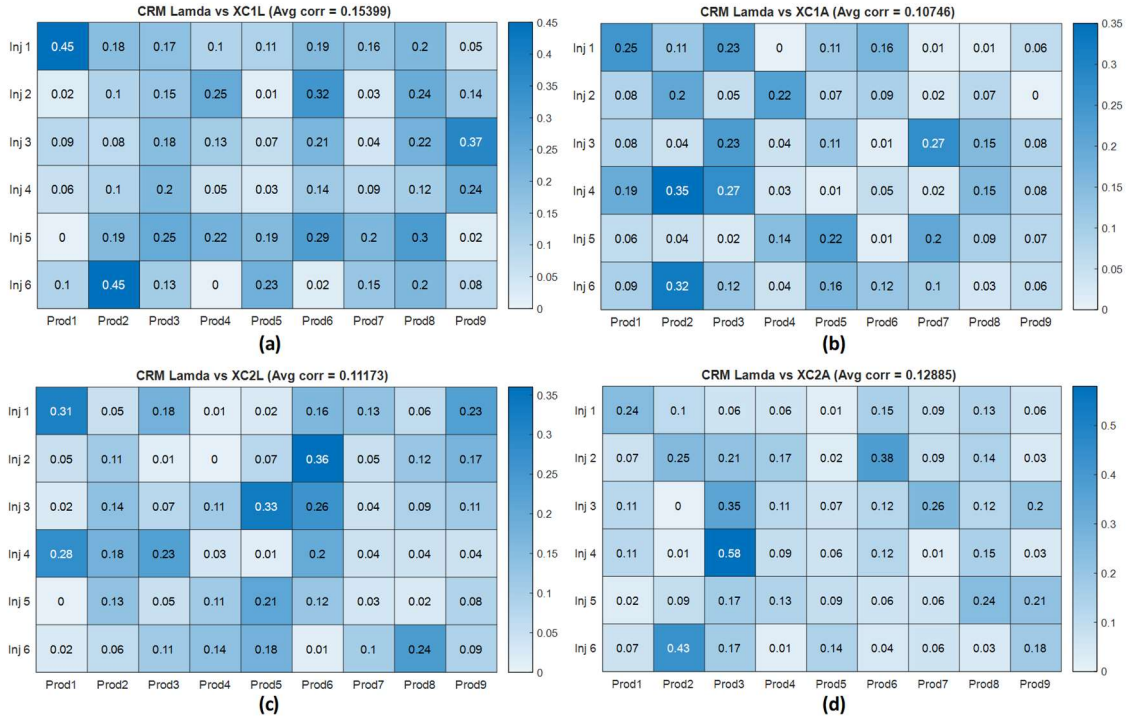

Figure 51. Heatmaps of the correlation coefficient of the scatter between capacitance-resistance model (CRM)-based weight coefficients and the proposed indicators based on cross-correlation coefficients using negative time-shifts. (a) CRM-based weight coefficients vs XC1L; (b) CRM-based weight coefficients vs XC1A; (c) CRM-based weight coefficients vs XC2L; (d) CRM-based weight coefficients vs XC2A.

Chapter 8: Discussions and Conclusions

Injector-producer connectivity and premature breakthrough of injected water or gas are persistent issues that can make or break the economics of secondary and tertiary recovery projects. In this thesis, I propose several connectivity measures and systematically evaluate their efficacy in characterizing subsurface connectivity picture. Due to the complexity of the reservoir and well-operating conditions, and the ever-evolving dynamics during secondary and tertiary recovery processes, it is hard to determine the connectivity between the injector and producer. Interestingly, CRM, one of the recent mainstream methods for well connectivity, fails to provide a consistent characterization of interwell communication. The proposed connectivity indicators based on signal-processing methods yield measures reasonably well even with evolving dynamics over the life of the field, as validated by streamline injector-producer pairwise allocation fractions.

The data required to determine the proposed connectivity indicators do not exclude transient data. However, we must note that data containing extreme spikes can introduce noises to the signals and may lead to biased results. In comparison to other methods, I believe the proposed connectivity indicators can provide realistic connectivity assessment. Another desirable feature of these methods is the simplicity and the fast calculation not involving solutions of complex model-based solutions of sets of partial differential equations. Nature is simple and complex in the same vein. No matter how sophisticated the system of equations we can devise and solve, we cannot adequately determine all the forces in nature. There will always be limitations in our solutions. The proposed connectivity measures are not based on an assumed model of relevance; rather it is based on “what the reservoir is telling us and how we heed to it.”

Nevertheless, the dynamic nature of reservoir requires the interwell connectivity picture to be described in an evolutionary manner. We cannot reflect the true dynamic of subsurface by using a single value to represent the communication between wells in the massive waterflood through years, as demonstrated in Figure 52. The picture shows simulated streamline at four time steps, indicating the dramatic changes of connections between wells. Compare the indicators to the mean value of these streamlines also leads to certain bias for the results.

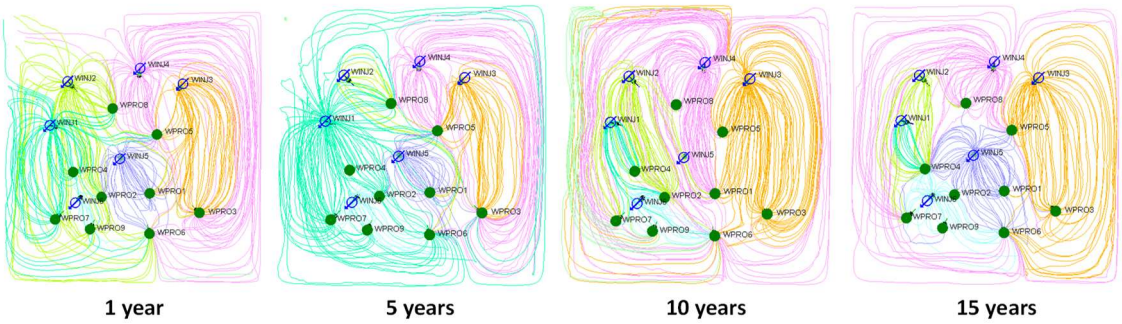

Figure 52. Example of simulated streamline evolution through time.

Future investigations into this approach will focus on finessing these indicators and their reliability under various reservoir conditions in a probabilistic framework. Use of these indicators in embedded virtual flow-metering applications will be explored in a future effort.

In this thesis, I have systematically evaluated and identified set of most realistic indicators that can resolve injector-producer distance effect, well interference effect, and multiwell reservoir complexities. Over 28 well-variable pairs and 12 connectivity indicators examined. The following conclusions appear pertinent:

1. I introduced several novel indicators of interwell connectivity based on signal-processing methods. They use standard well variables and their derivative

functions. Our investigation found indicators based on cross-correlation coefficients with negative time-shifts of the well-variable pair $F1 - F2$ to give the most significant and realistic connectivity information.

2. I assessed the quality of the proposed indicators by comparing against streamline-based injector-to-producer allocation fractions and capacitance-resistance model (CRM)-based weight coefficients. These indicators allow us to obtain connectivity information between injector-producer well pairs from the existing production and injection data and can track the connectivity picture over the life of the field.

Nomenclature

$F1$	modified production rate derivative
$F2$	injector-producer rate difference function
$q(t)$	production rate within time, can be water production rate, liquid production rate, oil production rate in STB/day, or reservoir volume production rate in RB/D
$i(t)$	injection rate within time, can be water injection rate in STB/D, or reservoir volume water injection rate in RB/D
t	discrete production time, month
J	productivity index, STB/D-psi
p_{wf}	bottom-hole pressure, psia
k_v	permeability in vertical direction, md
k_h	permeability in horizontal direction, md
R_{ip}	cross-correlation between injector and producer well pairs
s_t^i	discrete-time injector signals at time t
s_t^p	discrete-time producer signals at time t
C_{ip}	magnitude-squared coherence of the ith injector and pth producer
R_{ip}	cross-correlation between ith injector and pth producer well pairs
PSD_{ip}	cross power spectral density between ith injector and pth producer well pairs
PSD_i	power spectral density of the ith injector
PSD_p	power spectral density of the pth producer
$\widehat{Per}(f)$	normalized periodogram with frequency
N	number of data using in periodogram

References

Albertoni, A., and Lake, L. W. 2003. Inferring Interwell Connectivity Only From Well-Rate Fluctuations in Waterfloods. *SPE Reservoir Evaluation & Engineering*. February 2003: 6-16. doi:10.2118/83381-PA

Biterge, M. B., Hafez, H. H., Ouzzane, D., Khoury, J., and Safdar, M. 2014. Waterflood Surveillance in Lower Quality Carbonate Reservoir: History Matching of Fluid Front beyond Wellbore Using Deeplook Electromagnetic Time-Lapse Surveys. Society of Petrophysicists and Well-Log Analysts. Presented at the SPWLA 55th Annual Logging Symposium, Abu Dhabi, UAE, 18 – 22 May 2014.

Brigham, W. E., & Abbaszadeh-Dehghani, M. (1987, May 1). Tracer Testing for Reservoir Description. *Journal of Petroleum Technology*. May 1987: 519-527. doi:10.2118/14102-PA

Buck, J. R., Michael M. D., and Andrew C. S. 2002. *Computer Explorations in Signals and Systems Using MATLAB*. 2nd Edition. Upper Saddle River, NJ: Prentice-Hall.

Danaei, S., Hermana, M., and Ghosh, D. P. 2018. 4D Seismic Qualitative Interpretation for Water Injection Monitoring: Case Study in Southeast Asia. Presented at Offshore Technology Conference, Houston, TX, 30 April – 3 May 2018. doi:10.4043/28505-MS

Demiroren, A. N. 2007. *Inferring Interwell Connectivity from Injection and Productioin Data Using Frequency Domain Analysis*. M.S. thesis, Texas A&M University (May 2007).

De Sant Anna'Pizzaro, J.O. 1999. *Esitimating Injectivity and Lateral Autocorrelation in Heterogeneous Media*. PhD dissertation, The University of Texas at Austin (1999)

Dinh, A. V., and Tiab, D. 2008. Inferring Interwell Connectivity from Well Bottomhole Pressure Fluctuations in Waterfloods. *SPE Reservoir Evaluation & Engineering.* October 2008: 874-881. doi:10.2118/106881-PA

Heffer, K. J., Fox, R. J., McGill, C. A., & Koutsabeloulis, N. C. (1997, June 1). Novel Techniques Show Links between Reservoir Flow Directionality, Earth Stress, Fault Structure and Geomechanical Changes in Mature Waterfloods. *SPE Journal.* Volume 2, June 1997. doi:10.2118/30711-PA

Hou, J., Li, Z., Liu, Y., Zhang, Y., Wang, C., and Luo, F. 2011. Inferring Reservoir Interwell Dynamic Connectivity Based On Signal Processing Method. International Petroleum Technology Conference, Presented at the International Petroleum Technology Conference, Bangkok, Thailand, 7-9 February 2012. doi:10.2523/IPTC-14328-MS

Iman, R.L.; Davenport, J.M.; Zeigler, D.K. (1980). Latin hypercube sampling (program user's guide). OSTI 5571631

Izgec, O., & Kabir, C. S. (2009, January 1). Establishing Injector/Producer Connectivity Before Breakthrough During Fluid Injection. Presented at the SPE Western Regional Meeting, San Jose, California, 24-26 March 2009. doi:10.2118/121203-MS

Jansen, F. E., & Kelkar, M. G. (1997, January 1). Application of Wavelets to Production Data in Describing Inter-Well Relationships. Presented at the SPE Annual Technical Conference and Exhibition, San Antonio, Texas, 5-8 October 1997. doi:10.2118/38876-MS

Kim, J.K. 2011. *Development of Linear Capacitance-Resistance Models for Characterizing Waterflooded Reservoirs*. M.S. thesis, The University of Texas at Austin (December 2011).

Lee, J., Rollins, J.B. and Spivey, J.P. 2003. *Pressure Transient Testing.* SPE Textbook Series Volume 9, SPE, Richardson, TX, 2003.

Marfurt, K. J. (1984, January 1). Seismic Modeling: A Frequency-Domain/Finite-Element Approach. Presented at SEG Annual Meeting, Atlanta, Georgia, 2-6 December 1984.

Meyer, T. J. 2008. Monitoring Water Front Advancements with Down-hole Gravity Sensors. Presented at SEG Annual Meeting, Las Vegas, NV, 1 January 2008.

Mirzayev, M., and Jensen, J. L. 2016. Measuring Interwell Communication Using the Capacitance Model in Tight Reservoirs. Presented at SPE Western Regional Meeting, Anchorage, Alaska, 23-26 May 2015. doi:10.2118/180429-MS

Mirzayev, M., Riazi, N., Cronkwright, D., Jensen, J. L., and Pedersen, P. K. 2015. Determining Well-to-Well Connectivity in Tight Reservoirs, Presented at SPE/CSUR Unconventional Resources Conference, Calgary, AB, 20-22 October 2015. doi:10.2118/175943-MS

Morales, V. A., Ramirez, L. K., Garnica, S. V., Rueda, L. A., Gomez, V., Gomez, A., Bejarano, M. A. and Shook, G. M. 2018. Inter Well Tracer Test Results in the Mature Oil Field La Cira Infantas. Presented at the SPE Improved Oil Recovery Conference, Tulsa, OK, 14-18 April 2018. doi:10.2118/190315-MS

Ordonez Bustamante, A.C., Kabir, S., Reza, Z. 2018. Learning Reservoir Dynamics Metrics of Improved Oil Recovery Projects by Harnessing Real-Time Analysis and Data Analytics. Presented at the SPE Improved Oil Recovery Conference, Tulsa, OK, 14-18 April 2018. doi:10.2118/190206-MS

Panda, M. N., & Chopra, A. K. (1998, January 1). An Integrated Approach to Estimate Well Interactions. Presented at the SPE India Oil and Gas Conference and Exihibiioin, New Delhi, India, 17-19 February 1998. doi:10.2118/39563-MS

Poulsen, A., Shook, G. M., Jackson, A., Ruby, N., Charvin, K., Dwarakanath, V., Thach, S. and Ellis, M. 2018. Results of the UK Captain Field Interwell EOR Pilot. Presented at

the SPE Improved Oil Recovery Conference, Tulsa, OK, 14-18 April 2018. doi:10.2118/190175-MS

Prakasa, B., Shi, X., Muradov, K., & Davies, D. (2017, October 17). Novel Application of Capacitance-Resistance Model for Reservoir Characterisation and Zonal, Intelligent Well Control. Presented at the SPE/IATMI Pacific Oil & Gas Conference and Exibition, Jakarta, Indonesia, 17-19 October 2017. doi:10.2118/186277-MS

Refunjol, B.T., L.W. Lake 1999. Reservoir Characterization Based on Tracer Response and Rank Analysis of Production and Injection Rates. R. Schatzinger and J.Jordan, eds., *Reservoir Characterization – Recent Advances.* AAPG Memoir 71, p. 209-218

R.L. Plackett and J.P. Burman, "The Design of Optimum Multifactorial Experiments", Biometrika 33 (4), pp. 305–25, June 1946 doi:10.1093/biomet/33.4.305

Sayarpour, M. 2008. *Development and Application of Capacitance Resistive Models to Water/CO_2 Floods*. PhD dissertation, The University of Texas at Austin (August 2008).

Sayarpour, M., Kabir, C. S., and Lake, L. W. 2009. Field Applications of Capacitance-Resistive Models in Waterfloods. *SPE Reservoir Evaluation & Engineering.* December 2009: 853-864. doi:10.2118/114983-PA

Schlumberger. 2016. FRONTSIM technical reference manual. Houston, TX: Schlumberger.

Soeriawinata, T., & Kelkar, M. (1999, January 1). Reservoir Management Using Production Data. Presented at the 1999 SPE Mid-Continent Operation Symposiom, Oklahoma City, OK, 28-31 March 1999. doi:10.2118/52224-MS

Stoica, P., and Moses, R. 2005. *Spectral Analysis of Signals*. Upper Saddle River, NJ: Prentice Hall.

Tian, C., and Horne, R. N. 2016. Inferring Interwell Connectivity Using Production Data. Presented at the SPE Annual Technical Conference and Exhibition, Dubai, UAE, 26-28 September 2016. doi:10.2118/181556-MS

Tiong-Hui, W., and Cheng, S. T. Z. 2018. Decoding Interwell Tracer Data Using Novel Analytical Approach to Optimise Waterflood Management in a Complex Oil Rim Field, in Offshore East Malaysia. Presented at the Offshore Technology Conference, Kuala Lampur, Malaysia, 20-23 March 2018. doi:10.4043/28250-MS

Trauth, M. 2006. *MATLAB Recipes for Earth Sciences*. Berlin, Heidelberg: Springer Berlin Heidelberg.

Wilt, M., Zhang, P., Maeki, J., Netto, P., Queiroz, J. L. S., Santos, J. B., and Oliveira, V. 2012. Monitoring a Water Flood of Moderate Saturation Changes with Crosswell Electromagnetics (EM): A Case Study from Dom Joao Brazil. Presented at the SEG Annual Meeting, Las Vegas, NV, 4 November 2012.

Yousef, A. A., Gentil, P. H., Jensen, J. L., & Lake, L. W. (2005, January 1). A Capacitance Model to Infer Interwell Connectivity from Production and Injection Rate Fluctuations. Presented at the SPE Annual Technical Conference and Exhibition, Dallas, Texas, 9-12 October 2005. doi:10.2118/95322-MS

Yousef, A. A. 2006. *Investigating Statistical Techniques to Infer Interwell Connectivity from Production and Injection Rate Fluctuations*. PhD dissertation, The University of Texas at Austin (May 2006).

Zemel, B. 1995. Interwell Water Tracers. *Developments in Petroleum Science, Elsevier Science*. Volume 43, 1995: 89-135.